Draft version July 15, 2025
Typeset using LaTeX default style in AASTeX631

ALMA CMZ Exploration Survey (ACES) overview paper*

Steven N. Longmore [1,2] John Bally [3] Ashley T. Barnes [4] Cara Battersby [5] Laura Colzi [6]
Adam Ginsburg [7] Jonathan D. Henshaw [1,8] Paul Ho [9] Izaskun Jiménez-Serra [6]
J. M. Diederik Kruijssen [2] Elisabeth A.C. Mills [10] Maya Petkova [11] Mattia C. Sormani [12]
Robin G. Tress [13] Daniel L. Walker [14] Jennifer Wallace [5] Emad Alkhuja [15,16] Lucia Armillotta [17]
Nazar Budaiev [7] Rojita Buddhacharya [1] Alyssa Bulatek [7] Michael Burton [18]
Natalie O. Butterfield [19] Laura Busch [20] Paola Caselli [21] Mélanie Chevance [22,2] Claire Cook [23]
Enrico DiTeodoro [23] Simon R. Dicker [24] Katarzyna M. Dutkowska [25] Adam Fairley [26]
Christoph Federrath [27] Ruben Fedriani [28] Karl Fiteni [12,29] Gary Fuller [30] Pablo García [31,32]
Javier Goicoechea [33] Philipp Girichidis [34] Simon C. O. Glover [35] Mark Gorski [36] Savannah Gramze [7]
H. Perry Hatchfield [23] Rebecca Houghton [26] Pei-Ying Hsieh [37] Yue Hu [38] Mark Krumholz [39]
Alex Lazarian,[40] Laura McCafferty [26] Katharina Immer [4] Desmond Jeff [7,41] Janik Karoly [42]
Jens Kauffmann [43] Ralf S. Klessen [35,44,45,46] Emily M. Levesque [47] Fu-Heng Liang [48,49]
Dani Lipman [50] Xing Lu [51,52] Alessandro Lupi [23] S. Martín [53,54] Farideh Mazoochi [55]
Mark R. Morris [56] Marie Nonhebel [57] Francisco Nogueras-Lara [58] Tomoharu Oka [59]
Juergen Ott [60] Marco Padovani [61] Xing Pan [62,63,64] Jaime E. Pineda [21] Thushara G.S. Pillai [43]
Marc Pound [65] Denise Riquelme [66] Víctor M. Rivilla [67] Miguel Requena Torres [23] Galaxy Salo [26]
Álvaro Sánchez-Monge [68,69] Miriam G. Santa-Maria [7] Rainer Schoedel [28] Anika Schmiedeke [70]
Matthias Schultheis [71] Howard A. Smith,[72] Yoshiaki Sofue [73] Leonardo Testi [74] Grant R. Tremblay [75]
Gijs Vermariën [25] Alexey Vikhlinin [75] Arianna Vasini [76] Serena Viti [77] Q. Daniel Wang [78]
Fengwei Xu [79,80] Suinan Zhang [81] and Qizhou Zhang [64]

[1] *Astrophysics Research Institute, Liverpool John Moores University, IC2, Liverpool Science Park, 146 Brownlow Hill, Liverpool L3 5RF, UK*
[2] *Cosmic Origins Of Life (COOL) Research DAO, https://coolresearch.io*
[3] *Center for Astrophysics and Space Astronomy, Department of Astrophysical and Planetary Sciences University of Colorado, Boulder, CO 80389, USA*
[4] *European Southern Observatory (ESO), Karl-Schwarzschild-Straße 2, 85748 Garching, Germany*
[5] *Department of Physics, University of Connecticut, 196A Auditorium Road, Unit 3046, Storrs, CT 06269, USA*
[6] *Centro de Astrobiología (CAB), CSIC-INTA, Ctra. de Ajalvir Km. 4, 28850, Torrejón de Ardoz, Madrid, Spain*
[7] *Department of Astronomy, University of Florida, P.O. Box 112055, Gainesville, FL 32611*
[8] *Max Planck Institute for Astronomy, Königstuhl 17, D-69117 Heidelberg, Germany*
[9] *ASIAA*
[10] *Department of Physics and Astronomy, University of Kansas, 1251 Wescoe Hall Drive, Lawrence, KS 66045, USA*
[11] *Chalmers University*
[12] *Como Lake centre for AstroPhysics (CLAP), DiSAT, Università dell'Insubria, via Valleggio 11, 22100 Como, Italy*
[13] *Institute of Physics, Laboratory for Galaxy Evolution and Spectral Modelling, EPFL, Observatoire de Sauverny, Chemin Pegasi 51, 1290 Versoix, Switzerland*
[14] *UK ALMA Regional Centre Node, Jodrell Bank Centre for Astrophysics, The University of Manchester, Manchester M13 9PL, UK*
[15] *Max-Planck-Institut für Radioastronomie, Auf dem Hügel 69, 53121 Bonn, Germany*
[16] *Astronomy Department, Faculty of Science, King Abdulaziz University, P.O. Box 80203, Jeddah 21589, Saudi Arabia*
[17] *Princeton*
[18] *Armagh*
[19] *National Radio Astronomy Observatory, 520 Edgemont Road, Charlottesville, VA 22903, USA*
[20] *MPE*
[21] *Max-Planck-Institut für extraterrestrische Physik, Giessenbachstrasse 1, D-85748 Garching, Germany*
[22] *Universität Heidelberg, Zentrum für Astronomie, Institut für Theoretische Astrophysik, Albert-Ueberle-Str 2, D-69120 Heidelberg, Germany*
[23] *???*
[24] *Department of Physics and Astronomy, 209 S. 33rd Street, University of Pennsylvania, PA 19104, USA*

* Released on XXX, XXX, 202X

[25] *Leiden Observatory, Leiden University, P.O. Box 9513, 2300 RA Leiden, The Netherlands*
[26] *LJMU*
[27] *Research School of Astronomy and Astrophysics, Australian National University, Canberra, ACT 2611, Australia*
[28] *IAA*
[29] *Institute of Space Sciences & Astronomy, University of Malta, Msida MSD 2080, Malta*
[30] *Manchester University*
[31] *Chinese Academy of Sciences South America Center for Astronomy, National Astronomical Observatories, CAS, Beijing 100101, China*
[32] *Instituto de Astronomía, Universidad Católica del Norte, Av. Angamos 0610, Antofagasta, Chile*
[33] *CSIC*
[34] *University of Heidelberg*
[35] *Universität Heidelberg, Zentrum für Astronomie, Institut für Theoretische Astrophysik, Albert-Ueberle-Str. 2, 69120 Heidelberg, Germany*
[36] *North Western*
[37] *National Astronomical Observatory of Japan, 2-21-1 Osawa, Mitaka, Tokyo 181-8588, Japan*
[38] *Institute for Advanced Study, 1 Einstein Drive, Princeton, NJ 08540, USA*
[39] *ANU*
[40] *Department of Astronomy, University of Wisconsin-Madison, Madison, WI, 53706, USA*
[41] *National Radio Astronomy Observatory, 520 Edgemont Road, Charlottesville, VA 22903-2475, USA*
[42] *UCL*
[43] *Haystack Observatory, Massachusetts Institute of Technology, 99 Milsstone Road, Westford, MA 01886, USA*
[44] *Universität Heidelberg, Interdisziplinäres Zentrum für Wissenschaftliches Rechnen, Im Neuenheimer Feld 205, 69120 Heidelberg, Germany*
[45] *Harvard-Smithsonian Center for Astrophysics, 60 Garden Street, Cambridge, MA 02138, USA*
[46] *Elizabeth S. and Richard M. Cashin Fellow at the Radcliffe Institute for Advanced Studies at Harvard University, 10 Garden Street, Cambridge, MA 02138, USA*
[47] *Department of Astronomy, Box 351580, University of Washington, Seattle, WA 98195, USA*
[48] *Astronomisches Rechen-Institut, Zentrum für Astronomie der Universität Heidelberg, Mönchhofstraße 12-14, D-69120 Heidelberg, Germany*
[49] *European Southern Observatory, Karl-Schwarzschild-Straße 2, 85748 Garching, Germany*
[50] *University of Connecticut*
[51] *Shanghai Astronomical Observatory, Chinese Academy of Sciences, 80 Nandan Road, Shanghai 200030, P. R. China*
[52] *State Key Laboratory of Radio Astronomy and Technology, A20 Datun Road, Chaoyang District, Beijing, 100101, P. R. China*
[53] *European Southern Observatory, Alonso de Córdova, 3107, Vitacura, Santiago 763-0355, Chile*
[54] *Joint ALMA Observatory, Alonso de Córdova, 3107, Vitacura, Santiago 763-0355, Chile*
[55] *Institute for Research in Fundamental Sciences (IPM), School of Astronomy, Tehran, Iran*
[56] *Department of Physics & Astronomy, University of California, Los Angeles, Los Angeles, CA 90095-1547, USA*
[57] *St Andrews/ESO*
[58] *European Southern Observatory, Karl-Schwarzschild-Strasse 2, 85748 Garching bei München, Germany*
[59] *Department of Physics, Faculy of Science and Technology, Keio University, 3-14-1 Hiyoshi, Kohoku-ku, Yokohama, Kanagawa 223-8522, Japan*
[60] *NRAO*
[61] *INAF*
[62] *School of Astronomy and Space Science, Nanjing University, 163 Xianlin Avenue, Nanjing 210023, P.R.China*
[63] *Key Laboratory of Modern Astronomy and Astrophysics (Nanjing University), Ministry of Education, Nanjing 210023, P.R.China*
[64] *Center for Astrophysics | Harvard & Smithsonian, 60 Garden Street, Cambridge, MA, 02138, USA*
[65] *University of Maryland*
[66] *University of La Serena*
[67] *Centro de Astrobiología (CAB), CSIC-INTA, Carretera de Ajalvir km 4, Torrejón de Ardoz, 28850 Madrid, Spain*
[68] *Institute of Space Sciences (ICE, CSIC), Campus UAB, Carrer de Can Magrans s/n, 08193, Bellaterra (Barcelona), Spain*
[69] *Institute of Space Studies of Catalonia (IEEC), 08860, Barcelona, Spain*
[70] *Green Bank Observatory, P.O. Box 2, Green Bank, WV 24944, USA*
[71] *Nice*
[72] *Center for Astrophysics | Harvard & Smithsonian, 60 Garden Street, Cambridge, MA 02138*
[73] *Institue of Astronomy, The University of Tokyo, Mitaka, Tokyo, 181-0015, Japan*
[74] *ESO/Bologna*
[75] *Center for Astrophysics | Harvard & Smithsonian, 60 Garden St., Cambridge, MA 02138, USA*
[76] *University of Insubria*

[77] *Leiden Observatory, Leiden University, P.O. Box 9513, 2300 RA Leiden, The Netherlands*
and
Transdisciplinary Research Area (TRA) 'Matter'/Argelander-Institut für Astronomie, University of Bonn, Bonn, Germany
and
Department of Physics and Astronomy, University College London, Gower Street, London, UK
[78] *Department of Astronomy, University of Massachusetts, Amherst, MA 01003, USA*
[79] *Kavli Institute for Astronomy and Astrophysics, Peking University, Beijing 100871, People's Republic of China*
[80] *Department of Astronomy, School of Physics, Peking University, Beijing, 100871, People's Republic of China*
[81] *Nanjing*

ABSTRACT

The mass flows and energy cycles within the inner regions of galaxies exert a powerful influence on the evolution of the galaxy population. The centre of the Milky Way is the only galactic nucleus for which it is possible to resolve the physical mechanisms that drive these cycles, namely star formation and feedback, while also tracing global ($\gtrsim$100 pc) processes which determine where and when star formation and feedback occur. We present an overview of ACES, the 'ALMA CMZ Exploration Survey', an ALMA Band 3 survey of the 'Central Molecular Zone' (CMZ) – the inner-100 pc of the Galaxy (l = 359.4° to 0.8°). ACES spectral setup is tuned to observe optimal tracers of the physical, chemical, and kinematic conditions in as many as 71 spectral features (e.g. HCO^+, HNCO, SiO, H40α, complex molecules) of the gas in the CMZ, to derive the properties of all potentially star-forming Galactic Centre gas, from global (100 pc) to proto-stellar core (0.05 pc) scales, down to sub-sonic ($<$0.4 km s^{-1}) velocity resolution. In this overview paper, we provide the scientific justification for the ACES survey, explain the choice of observational setup, and describe the anticipated data legacy products. Finally, we show some of the initial ACES data which highlight the power of ACES' combination of high angular resolution, unprecedented spatial dynamic range, sensitivity, spectral resolution and spectral bandwidth as an illustration of how ACES aims to understand how global processes set the location, intensity, and timescales for star formation and feedback in the CMZ.

Keywords: Central Molecular Zone — Galactic Center — ISM: kinematics and dynamics — ISM: molecules — Star formation — Surveys

1. INTRODUCTION

The mass flows and energy cycles in galactic nuclei play a key role in shaping the evolution of the galaxy population (e.g., Veilleux et al. 2005; Cicone et al. 2014; Heckman & Best 2014; Harrison 2017). Bars and other large-scale stellar structures, as well as molecular clouds and star-formation complexes, evolve from these flows and cycles, both baryonic and radiative, and from historical gravitational processes including galaxy mergers. The central regions of galaxies are thus key to understanding these multiple cycles, evolutionary histories, and to quantifying how these global processes determine the location, intensity, and timescales for star formation and feedback. (Henshaw et al. 2023). It is clear that many processes are involved – a deep gravitational potential well, rapid differential rotation, turbulence injection, shocks, strong magnetic fields, etc. (Kruijssen et al. 2014; Krumholz & Kruijssen 2015; Krumholz et al. 2017; Federrath et al. 2016; Sormani & Barnes 2019; Sormani et al. 2020; Hatchfield et al. 2021) – the effects of which cascade from global (100 pc), to cloud (few to 10 pc), to prestellar core (0.05 pc) scales (Longmore et al. 2013a; Walker et al. 2015, 2018; Henshaw et al. 2016; Kruijssen et al. 2019; Battersby et al. 2024). The centre of our Galaxy is the only nucleus for which we can resolve the physics of star formation and feedback down to the scale of individual protostellar cores (e.g. Ginsburg et al. 2018; Lu et al. 2020, 2021; Walker et al. 2021; Zhang et al. 2025; Xu et al. 2025), thereby providing the crucial link between galactic-scale processes and the small-scale physics that ultimately regulate star formation and feedback (Molinari et al. 2011; Longmore et al. 2013b; Kruijssen et al. 2014; Henshaw et al. 2023).

Determining the relative importance of these processes as a function of spatial scale, time and location requires measuring the physical and kinematic properties of gas contiguously over all these scales and comparing the gas properties with the comparatively well-established distribution of young stars and other feedback sources (Fig. 1). Previous single-dish observations have inadequate spatial resolution to achieve this goal (e.g., Jones et al. 2012; Walsh

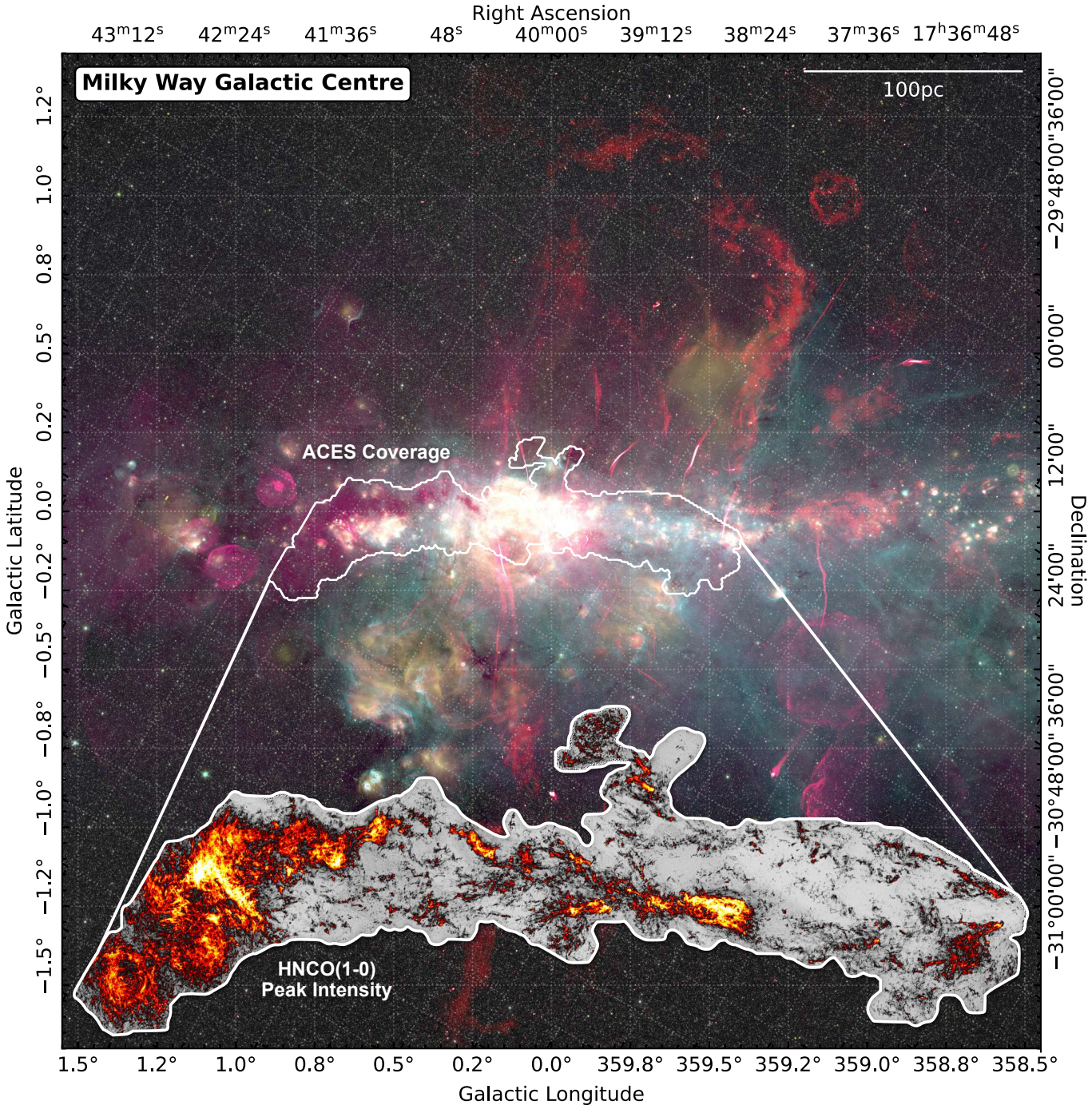

Figure 1. Finding chart for the Galactic Center. A colour composite of the 4.5 μm (white) and 8 μm (green) emission from the Spitzer GLIMPSE survey (Churchwell et al. 2009), 24 μm (yellow) emission from the Spitzer MIPSGAL survey (Carey et al. 2009), and 20 cm (red) emission observed by MeerKAT (Heywood et al. 2019, 2022) and the Green Bank Telescope (GBT; Law et al. 2008). Overlaid as a white contour is the coverage of the ACES survey (see Fig. 2). The inset zoom-in shows the ACES HNCO(1-0) peak intensity map. The background image of this Figure is adapted from Henshaw et al. (2023). See Fig. 11 for a labeled version, highlighting several features of interest across the Galactic Centre.

et al. 2011; Purcell et al. 2012; Ginsburg et al. 2016; Krieger et al. 2017), and existing interferometric studies at the targeted resolution are restricted to individual clouds (e.g., Battersby et al. 2020, see Fig. 2). This discontinuity in spatial dynamic range leaves us with a fundamental gap in our knowledge between the small-scale physics of star formation and the global (∼100 pc) processes that control it. The goal of the ALMA CMZ Exploration Survey

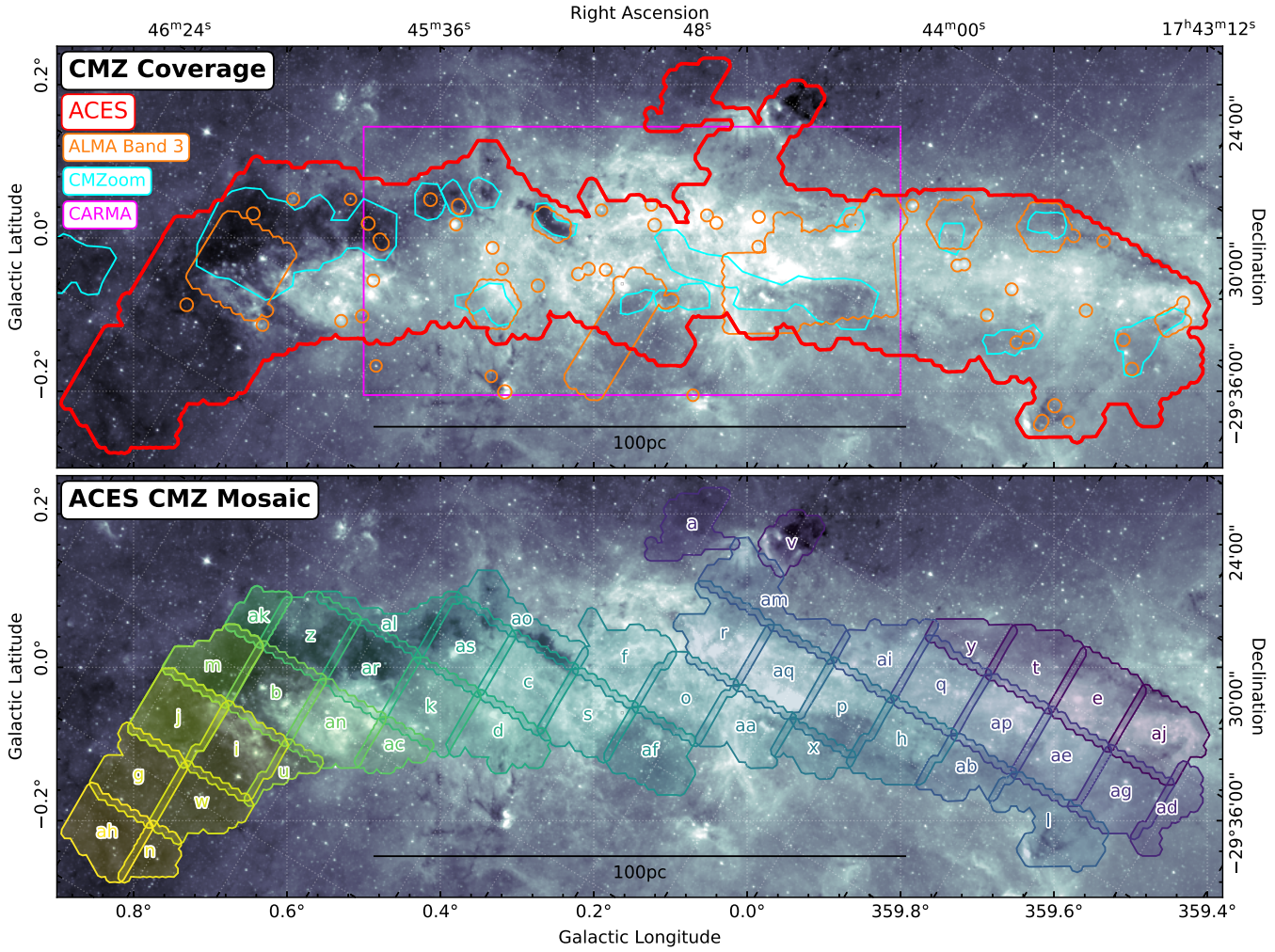

Figure 2. Coverage of the ACES survey. The upper panel displays the spatial coverage of the ACES survey, indicated by the red contour (see also Fig. 1). Overlaid orange contours denote the pre-ACES archival observations available in ALMA Band 3. The outline of the SMA 1 mm CMZoom survey (Battersby et al. 2020; Hatchfield et al. 2020; Callanan et al. 2023) is shown as the cyan contour, while the magenta rectangle represents the coverage of the CARMA survey (Pound & Yusef-Zadeh 2018). The lower panel presents the individual mosaics comprising the ACES survey, each labelled with an alphabetical identifier. Both panels are superimposed on the *Spitzer* 8 μm image from the GLIMPSE survey (Churchwell et al. 2009).

(ACES) is to move beyond comparing a small number of the highest density gas clouds with inhomogeneous sensitivity, resolution and spectral setups, to building a global understanding of star formation, feedback, and the mass flows and energy cycles across the whole Central Molecular Zone.

In this ACES overview paper, we describe the ACES scientific context and survey design. In Section 2, we explain the observational strategy, including the choice of tracers, spectral setups, and angular resolution that together provide the means to connect the large-scale mass flows with the formation of dense, star-forming cores. In Section 3 we describe the complementary unified simulations framework developed to aid the interpretation of the data. Sections 4 and 5 describe the science objectives and the open science approach, respectively. Finally, in Section 6 we show some of the initial ACES data which highlight the power of ACES' combination of high angular resolution, unprecedented spatial dynamic range, sensitivity, spectral resolution and spectral bandwidth as an illustration of how ACES aims to understand how global processes set the location, intensity, and timescales for star formation and feedback in the CMZ.

In a series of companion papers, we present the ACES continuum data (Ginsburg & ACES Team 2025), the high spectral resolution (0.2 km s^{-1}) HNCO & HCO$^+$ data (Walker & ACES Team 2025), the two intermediate spectral

resolution (1.7 km s^{-1}) windows, containing SiO (2−1), SO (22−11), H^{13}CO$^+$ (1−0), H^{13}CN (1−0), HN^{13}C (1−0), and HC^{15}N (1−0) (Lu & ACES Team 2025), and the two broad spectral windows containing CS(2−1), SO (23 − 12), CH_3CHO 5(1,4) − 4(1,3), HC_3N(11−10) and H40α (Hsieh & ACES Team 2025). We request that anyone using ACES data, please cite the relevant papers containing that data.

2. THE ALMA CMZ EXPLORATION SURVEY (ACES): OBSERVATIONAL DESIGN

The Atacama Large Millimeter/submillimeter Array (ALMA) CMZ Exploration Survey (ACES) Large Program (Project code: 2021.1.00172.L; PI: S. Longmore) provides uniform Band 3 coverage of the inner $1.5^\circ \times 0.5^\circ$ of the CMZ. ACES top-level observational goal was to achieve a uniform 1.5″ (∼0.05 pc) angular resolution, Band 3, molecular line and dust continuum survey of all gas in the inner 100 pc of the Galaxy dense enough to form stars, at a line sensitivity of 1 K (∼32 mJy/beam) per 0.2 kms^{-1} channel and a continuum sensitivity of 0.07 mJy beam^{-1}, covering the full range of CMZ gas velocity ($V_{LSR}\pm \sim 150$ km s^{-1}). In practice, due to the broad spectral windows used in most of the correlator settings, the velocity range for all lines other than HNCO and HCO$^+$ in the narrow spectral window extends far beyond $V_{LSR}\pm \sim 150$ km s^{-1} in all spectral lines.

The definition of the ACES survey area was driven by the fundamental requirement to cover all gas in the inner ∼100 pc of the Galaxy expected to form stars. To meet this requirement, the survey area was defined to include all gas above a column density threshold of 10^{22} cm^{-2} (based on the column density maps from Battersby et al. 2024; Fig. 2) – the column density of gas above which stars are observed to form in the Galactic disc (e.g Lada et al. 2012). This choice of column density threshold allows a direct comparison between star-forming gas in the CMZ with the disc of the Milky Way and other galaxies, making it possible to quantify the impact that the Galactic environment has on the star formation process.

The survey area imposed by the column density threshold of 10^{22} cm^{-2} required making the largest contiguous map on the sky that ALMA has ever made. The survey area is broken up into 45 contiguous regions following an alphabetised naming convention randomised from ‘a’ to ‘as’ containing up to 150 pointings per observation (Fig. 2).

The large survey area was a limiting factor in the choice of the spectral setup. At the time of the ACES observations, only Band 3 had a sufficiently large primary beam to mosaic the survey area within the observational time constraints. The Band 3 spectral setup was selected to contain transitions with critical density and excitation energy ranges to trace the gas kinematic, physical, and chemical properties from global (tens of pc), to cloud (few pc), to core (0.05 pc) scales (see Table 1 for an overview of the spectral setup, and Table 2 for a list of spectral lines in the observed frequency ranges).

Two high spectral resolution (0.2 km s^{-1}) windows centred on the reliable gas kinematic tracers HCO$^+$ and HNCO (Henshaw et al. 2016; He et al. 2021) were chosen to resolve the thermal linewidth (0.4 km s^{-1} in the 60 K CMZ gas; Ginsburg et al. 2016; Krieger et al. 2017) in global-to-cloud and cloud-to-core scale gas, respectively. Due to the narrow bandwidth in these high spectral resolution windows, the central frequency needed to be shifted as a function of spatial position to make sure the corresponding V_{LSR} range encompassed the CMZ gas velocities (between ±150 km s^{-1}).

The other four spectral windows cover observed frequencies 85.96–86.43 GHz (SPW 25, resolution of 1.7 km s^{-1}), 86.67–87.13 GHz (SPW 27, resolution of 1.7 km s^{-1}), 97.66–99.54 GHz (SPW 33, resolution of ∼3 km s^{-1}), and 99.56–101.44 GHz (SPW 35, resolution of ∼3 km s^{-1}). The two intermediate spectral resolution (1.7 km s^{-1}) windows centred on dense gas and shock tracers and their isotopologues were chosen to trace gas kinematics in intermediate density gas and solve degeneracies in opacity and excitation. The ^{13}C, ^{18}O, and ^{15}N isotopic substitutions of HCO$^+$, HCN, and HNC trace stellar nucleosynthesis gas enrichment (Riquelme et al. 2010) and the properties of increasingly higher density (smaller scale) gas when the main isotope transitions become optically thick. Other lines were chosen to trace specific physical processes and regimes, such as shocks (SiO), cosmic ray irradiation and star formation activity (e.g., HC_5N, HC_3N), ionised gas (H40α, H50β) and chemical complexity (complex organic molecules). Finally, two broad bands were selected with 2.9 km s^{-1} resolution, sufficient to trace the bulk kinematics and chemical complexity while allowing removal of lines to obtain continuum measurements. The bandwidth of the intermediate and broad spectral windows correspond to velocities of many thousands of km s^{-1}, easily sufficient to encompasses all the CMZ gas velocities.

ACES’ targeted angular resolution of 1.5″ (0.05 pc) was chosen to match the expected size of dense (pre)star-forming cores in CMZ clouds (Ginsburg et al. 2018). Additional 7m ACA and total power observations were conducted to recover emission from large spatial scales for the line data, as existing single-dish data do not cover the full ACES

Table 1. Overview of the ACES spectral configuration. Shown for each 12m spectral window (SPW) ID are the lower ($\nu_{\rm L}$) and upper ($\nu_{\rm U}$) frequency bounds, native channel widths ($\Delta\nu$), and bandwidth. Prominent lines in each SPW are also shown.

SPW	$\nu_{\rm L}$	$\nu_{\rm U}$	$\Delta\nu$	Bandwidth	Prominent Lines
	GHz	GHz	km s^{-1}	GHz	
25	85.9656	86.4344	0.849	0.46875	HC^{15}N 1-0, SO 2_2-1_1, SiO 2-1 v=1 maser, H^{13}CN 1-0
27	86.6656	87.1344	0.842	0.46875	H^{13}CO+ 1-0, SiO 2-1, HN^{13}C 1-0
29	89.1592	89.2178	0.103	0.05859	HCO$^+$ 1-0
31	87.8959	87.9545	0.104	0.05859	HNCO 4-3
33	97.6625	99.5375	1.485	1.875	CS 2-1, CH_3CHO 5(1,4)–4(1,3) A–, H40α, SO 2_3-1_2
35	99.5625	101.438	1.457	1.875	HC_3N 11-10

spectral window and suffer from artifacts in large spatial and frequency ranges (Jones et al. 2012). Single-dish data from the Mustang Galactic Plane Survey (Ginsburg et al. 2020) provide the 3mm continuum zero-spacing flux.

Based on the observed brightness temperatures in existing single-dish data (Jones et al. 2012), previous ALMA observations of CMZ clouds at a similar resolution and sensitivity, and numerical simulations with chemistry and radiative transfer modelling (Petkova et al. 2023a), ACES targeted a line sensitivity of RMS = 1.0, 0.6 and 0.25 K in 0.2, 1.7 and 3 km s^{-1} channels, respectively, to detect all key lines necessary to achieve ACES' science goals at high significance in essentially all pointings. The corresponding continuum sensitivity of 0.07 mJy beam^{-1} is sufficient to detect $\sim$10 M$_\odot$, 30 K cores at 5σ. As ACES is able to detect all cores more massive than $\sim$10 M$_\odot$, it therefore provides a complete census of all precursors of high-mass stars in the CMZ. The corresponding column density sensitivity of $\sim10^{22}$ cm^{-2} matches the column density threshold used to define the survey area.

Full details of the data reduction are given in the corresponding companion papers (Ginsburg & ACES Team 2025; Walker & ACES Team 2025; Lu & ACES Team 2025; Hsieh & ACES Team 2025).

3. THE ALMA CMZ EXPLORATION SURVEY (ACES): UNIFIED SIMULATION NETWORK

It was clear from the initial conception of the survey design, that a complementary suite of numerical simulations able to self-consistently trace the baryon cycle as well as gas dynamics and star formation at the same spatial scales as the ACES observations were a crucial component of achieving the core science objectives. With appropriate post-processing to produce accurate synthetic images, the simulation parameter space study aims to provide the necessary statistical framework to interpret the key physical agents (gravitational forces, rapid differential rotation, turbulence injection, shocks, strong magnetic fields, etc.,) controlling the evolution from global (100 pc), to cloud (few to 10 pc), to prestellar core (0.05 pc) scales.

Due to the large spatial dynamic range of the gas flow and star formation within the Galactic Centre, we have chosen to address the modelling through a multi-scale framework of numerical simulations. We use these simulations as numerical experiments in which we control the physical assumptions in order to constrain the effects and importance of various mechanisms (such as magnetic fields, stellar feedback, etc.). On the largest scales, we model the Galactic bar through the inclusion of a Milky-Way-like gravitational potential (Hunter et al. 2024). This creates a continuous flow of gas towards the Galactic Centre and results in the self-consistent formation of a CMZ-like region (see panels A and B in Figure 3). These large-scale simulations are used for studying the time-evolution of the gas in the region as a whole and help interpret its complex 3D geometry. They may also identify sites where increased star formation might be expected, however they cannot resolve the formation of individual stars. Some recent examples of such simulations include Sormani et al. (2020), Tress et al. (2020), and Hatchfield et al. (2021), with Petkova et al. (2023a), Petkova et al. (2023b) and Tress et al. (2024) largely developed as part of the ACES project.

On the other side of the size scale we have simulations of individual clouds on CMZ orbits through the Galactic Centre gravitational potential (e.g. Dale et al. 2019; Kruijssen et al. 2019, see panel C of Figure 3). Such simulations can resolve star formation and test the physical mechanisms that affect it on a small scale. They can also be set up to match properties of known clouds (e.g., Clark et al. 2013), and attempt to reproduce their observed morphology, especially after being post-processed with radiative transfer (panel D of Figure 3). However, these models do not include interactions between the clouds, and are more suitable for clouds that can be treated as individual entities. Some recent examples of analysis of these simulations include Petkova et al. (2023a) and Petkova et al. (2023b).

Table 2. Simple molecules included in the ACES setup. The transitions, rest frequencies and corresponding SPW are given.

Molecule	Transition	Rest Frequency(GHz)	12m SPW
$HC^{15}N$	1-0	86.0549	25
SO	2(2)-1(1)	86.0939	25
CCS	7(6)-6(5)	86.1813	25
SiO v=1 maser	2-1	86.2434	25
$H^{13}CN$	1-0	86.33992	25
HCO	1(0,1,2,1)-1(0,0,1,0)	86.7083	27
$H^{13}CO^+$	1-0	86.7543	27
HCO	1(0,1,1,1)-1(0,0,1,1)	86.7774	27
HCO	1(0,1,1,0)-1(0,0,1,1)	86.8057	27
SiO v=0	2-1	86.8469	27
$HC^{17}O^+$	1-0	87.0575	27
$HN^{13}C$	1-0	87.0908	27
HNCO	4-3	87.9252	31
HCO^+	1-0	89.1885	29
^{34}SO	2(3)–1(2)	97.7153	33
CS	2-1	97.9809	33
^{33}SO	2(3,4)-1(2,3)	98.4892	33
^{33}SO	2(3,5)–1(2,4)	98.4936	33
HC_5N	37–36	98.5125	33
C_3N	10(11)-9(10)	98.940	33
C_3N	10(10)-9(9)	98.958	33
H40α		99.02295	33
H50β		99.22521	33
SO	2(3)-1(2)	99.2999	33
$HC^{13}CCN$	11-10	99.6518	35
$HCC^{13}CN$	11-10	99.6615	35
$H_2C^{34}S$	3(1,3)–2(1,2)	99.7740	35
CCS	8(7)-7(6)	99.8665	35
$S^{18}O$	3(2)–2(1)	99.8038	35
SO	5(4)–4(4)	100.0296	35
HC_3N	11-10	100.0764	35
HC_5N	38–37	101.1747	33
NS^+	2–1	100.1985	35
HC_3N, v6=1	11(1)-10(-1)	100.2406	35
$H_2C^{34}S$	3(0,3)–2(0,2)	101.2843	35
HC_3N, v6=1	11(-1)-10(1)	100.3194	35
HC_3N, v7=1	11(1)-10(-1)	100.3224	35
HC_3N, v7=1	11(-1)-10(+1)	100.46617	35
CH3NC	5(1)–4(1)	100.5242	35
CH3NC	5(0)–4(0)	100.5265	35
HC_3N v7=2	11(0)-10(0)	100.70878	35
HC_3N v7=2	11(2)-10(-2)	100.71106	35
HC_3N v7=2	11(-2)-10(2)	100.71439	35
$H_2C^{34}S$	3(0,3)–2(0,2)	101.2843	35
H_2CO	6(1,5)–6(1,6)	101.332987	35

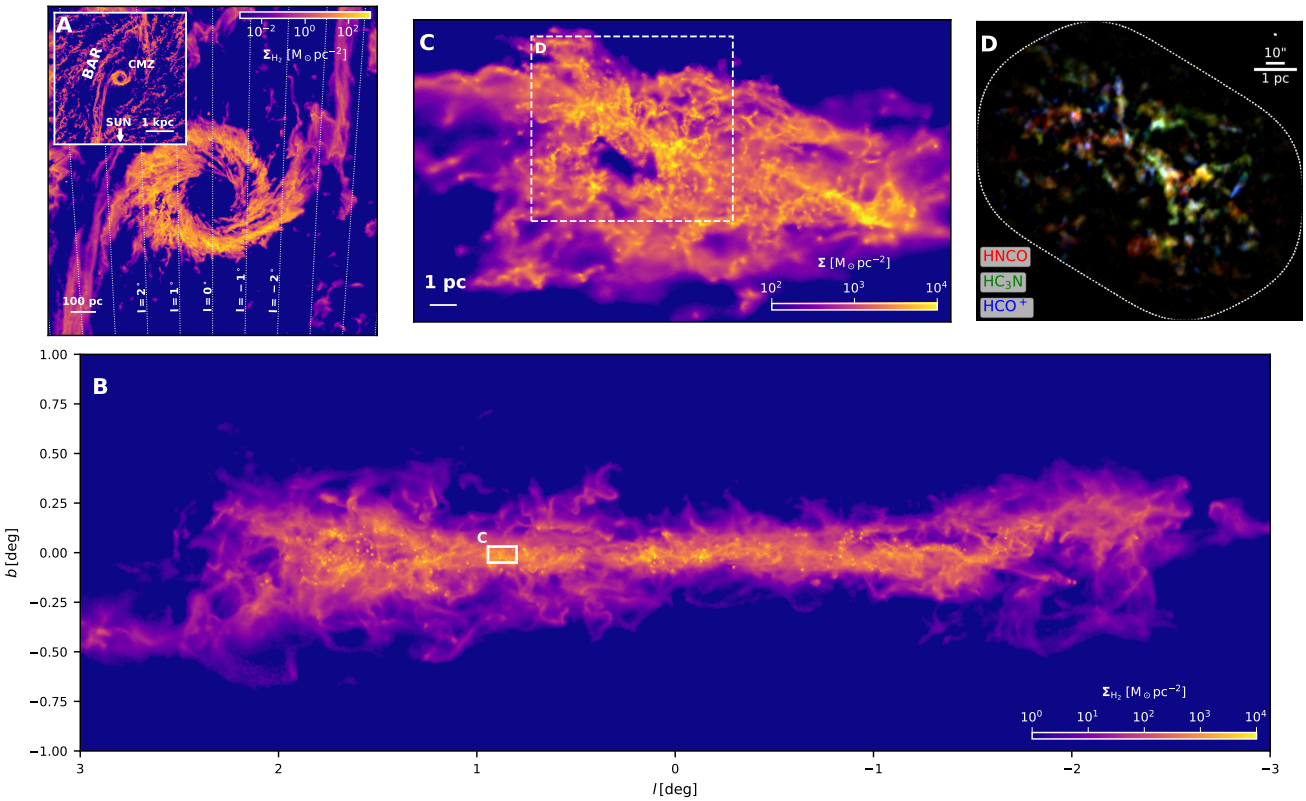

Figure 3. Example of simulations in development that will help with interpretation of ACES data. White boxes illustrate zoom-in regions in other panels. *Panels A-B*: a top-down and plane-of-the-sky projection of a large-scale simulation of the gas flow in the Galactic bar with star formation, stellar feedback (supernovae, ionising radiation) and magnetic fields (ideal MHD). Simulations like this one can follow the formation of the CMZ and of individual molecular clouds self-consistently from kpc scales down to the cloud scale, but cannot resolve star formation. *Panel C:* simulation of an individual molecular cloud on a CMZ orbit through the Galactic potential, that can resolve star formation (Adapted from Dale et al. 2019; Kruijssen et al. 2019). *Panel D:* a synthetic line emission image created by post-processing the simulation snapshot from Panel C (Adapted from Petkova et al. 2023a).

In addition to the separate large-scale and small-scale simulations, the development of high-resolution zoom-in simulations are important for bridging the gap between Galaxy-scale dynamical evolution and individual star forming regions (e.g. Hatchfield et al. 2021; Lipman et al., in prep). These zoom-ins aim to incorporate as much key physics as possible (e.g. up-to-date Galactic potential, magnetic fields, star formation and feedback, etc) to simulate the large-scale Galactic environment, while also reaching resolutions in the CMZ to resolve individual molecular clouds with star forming cores.

Section 6.1 describes dedicated astrochemistry models that are being developed to interpret the plethora of lines detected with ACES. These high chemical fidelity models naturally complement the above hydro simulations, which contain a lot of physics but only very simplified chemistry.

4. ACES SCIENCE OBJECTIVES

Gas flows in the inner kpc of the Milky Way are typical of those in other barred-spiral galaxies (Binney et al. 1991; Rodríguez-Fernández & Combes 2008; Tress et al. 2020; Stuber et al. 2023). Gas, funnelled radially inward from the disk, builds up a massive (few $10^7\,M_\odot$), dense ($10^4\,cm^{-3}$) gas stream orbiting the centre ($r \sim 100\,pc$; Bally et al. 2010; Molinari et al. 2011; Kruijssen et al. 2015). Empirical star formation relations relating the amount of dense gas to the star formation rate predict this gas should be producing $\sim 1\,M_\odot\,yr^{-1}$ of stars (Longmore et al. 2013b), yet the star formation rate has been constant at $\lesssim 0.1\,M_\odot\,yr^{-1}$ to within a factor 2 for the last $\sim$5–10 Myr (Barnes et al. 2017; Elia et al. 2025). This poses fundamental problems for star formation theories given that the free-fall time and turbulence dissipation timescale are both only $\sim$1 Myr. Theory, numerical simulations, and pilot studies of individual clouds all show that global ($\lesssim$100 pc) gas dynamics play a fundamental role in determining the star formation activity (or lack

thereof) throughout the CMZ (Kruijssen et al. 2014; Rathborne et al. 2015; Federrath et al. 2016; Sormani et al. 2020). With observations of transitions covering the required critical densities and excitation energies, ACES aims to provide the mass distribution and velocity structure at a contiguous spatial dynamic range of $\approx 10^4$, down to proto-stellar core scales. Combined with a suite of complementary numerical simulations, this crucial global-to-protostellar link overcomes the fundamental challenge of existing studies, making it possible to achieve ACES' core aim of quantifying how global (~ 100 pc) processes determine the location, intensity, and timescales for star formation and feedback. This core goal is split into four science objectives.

4.1. *Science Objective 1: Determine the mechanisms driving mass flows as a function of size scale and location*

Comparing the observed mass distribution and kinematic structure with numerical simulations of gas evolving in the known gravitational potential, ACES aims to determine the relative influence of different physical processes (orbital motion, shear, turbulence, mass accretion, etc.) in shaping the proto-stellar core (0.05 pc) scale physical structure and internal dynamics of gas clouds, as a function of location across the CMZ (Kruijssen et al. 2019; Dale et al. 2019; Sormani et al. 2020; Tress et al. 2020). With a measure of the kinetic energy density as a function of size-scale and position, ACES aims to (i) test the relative importance of different energy injection mechanisms (e.g. shear) and how this in turn determines the location and magnitude of star formation (e.g., Klessen & Glover 2016); (ii) correlate the molecular and ionised gas properties with the known sources of feedback (e.g. Barnes et al. 2020) to measure the momentum and energy injection interior and exterior to clouds (Kruijssen et al. 2014, 2019; Federrath et al. 2016; Henshaw et al. 2016).

4.2. *Science Objective 2: Disentangling the 3D CMZ geometry*

The CMZ is one of the most well-studied regions in astrophysics, with ongoing or recently completed large programs across the electromagnetic spectrum on MeerKAT, VLA, SMA, SOFIA, VLT, XMM-NEWTON, Chandra, etc. CMZ studies have produced many exciting results, e.g., key tests of general relativity (GRAVITY Collaboration et al. 2018), and the centre of the Galaxy remains an optimal location for testing physics in extreme environments, e.g. searching for evidence for annihilating dark matter (Murgia 2020). However, the potential of the CMZ as a laboratory of extreme physics is fundamentally limited by the fact that observations only provide a 2D projection of the complex interplay of different physical processes. The inability to determine the location and motions of gas and young stars across the CMZ is the limiting factor in interpreting the large volumes of observational data attempting to use the Galactic Centre to tackle fundamental questions such as the nature of dark matter.

A major source of contention in the literature is not knowing which clouds belong to the stream of gas that orbits the Galactic centre at a radius of $\sim$100 pc. Current single-dish data cannot spatially resolve overlapping components of the stream structures, and are too coarse for comparison with X-ray studies which could provide line-of-sight gas locations (Terrier et al. 2018). Interferometric studies do not have the field of view or sensitivity to trace the gas in between the clouds. Our present view of clouds as 'isolated islands' means we cannot distinguish whether they lie close to the centre and are in the process of feeding the next major supermassive blackhole accretion event, or lie at Galactocentric radii of $\lesssim$100 pc and are about to form a new generation of super star clusters. ACES' ability to trace the contiguous position-position-velocity structure, combined with the simulation framework, will build upon our evolving understanding of the 3D gas geometry (Battersby et al. 2025a,b; Walker et al. 2025; Lipman et al. 2025) and help to break the remaining degeneracies (e.g. Henshaw et al. 2016), leading to a unified picture of the 3D gas structure with enormous legacy value for future studies.

4.3. *Science Objective 3: Determine if there are preferred locations for star formation in the CMZ*

Studies of extragalactic CMZs show there may be preferred locations at which gas clouds transition from quiescent to star-forming (Böker et al. 2008). In one scenario, star formation can be triggered at the contact point between the dust lanes feeding the nuclear ring and the ring itself (Böker et al. 2008; Seo & Kim 2013; Sormani et al. 2020). In the CMZ, it has been argued that star formation may also be coordinated and triggered by tidal compression of clouds passing pericentre with the bottom of the Galactic gravitational potential (Longmore et al. 2013a; Kruijssen et al. 2015). The former scenario applied to the CMZ would predict star formation activity and properties of the embedded cores depend on where infalling gas collides with existing gas clouds (at Sgr B2 and Sgr C located at apocentre; Bally et al. 2010). The latter predicts increasing star formation as clouds progress farther downstream from pericentre passage. With a measure of the embedded star formation (e.g. Lu et al. 2019) crucially now complete as a function of

location, and with a complete description of the gas distribution, ACES aims to distinguish between these predictions and provide critical insight into the formation of super star clusters and the central starburst activity that plays a key role in galaxy evolution (e.g. Leroy et al. 2018).

4.4. *Science Objective 4: Determine whether star formation theory predictions hold in extreme environments*

Theories combining the scale-free physics of turbulence with gravity in a multi-freefall framework (Mac Low & Klessen 2004a; McKee & Ostriker 2007; Hennebelle & Chabrier 2011) predict star formation varies strongly with the virial parameter, $\alpha_{\rm vir}$, the turbulent Mach number, $\mathcal{M}$, and the driving mode of turbulence, b (e.g., Federrath & Klessen 2012). Specifically, in many of the modern theories of the star formation rate (SFR) and the initial mass function (IMF) the 'critical density' for star formation, $\rho_{\rm crit}$, is proportional to $\alpha_{\rm vir}\mathcal{M}^2$ (Krumholz & McKee 2005; Padoan & Nordlund 2011), and the peak and width of the pre-stellar core mass function and the IMF are set by the sonic scale, $R_{\rm S}$, where gravity overcomes thermal pressure (Hopkins 2013; Hennebelle & Chabrier 2013). With a measurement of the density and velocity field, ACES will provide the data to determine $\alpha_{\rm vir}$ and $\mathcal{M}$, as well as $\rho_{\rm crit}$ and $R_{\rm S}$ with unprecedented precision and coverage, enabling stringent tests of these predictions for all potentially star-forming gas in the CMZ (Bertram et al. 2015; Barnes et al. 2017). Compared to star formation regions in the Galactic disk, against which many of the star formation theories are calibrated, the density, velocity, and temperature are significantly different in the CMZ, leading to differences in $\rho_{\rm crit}$ and $R_{\rm S}$ by about an order of magnitude, owing to differences in key environmental properties such as the radiation field and cosmic-ray ionization rate. It is therefore critical to determine the dimensionless parameters $\alpha_{\rm vir}$, $\mathcal{M}$, and b, to test the theoretical predictions of star formation, and indeed some of these parameters may vary substantially in the CMZ, posing challenges for some of the theoretical models. ACES will provide a new benchmark for star formation theories in extreme environments similar to those in $z \sim 1$–3 galaxies and local starbursts (Kruijssen & Longmore 2013) at otherwise unreachable scales. With a complete census of core masses, velocities and velocity dispersions for high-mass star precursors, ACES will tackle fundamental open questions in star formation research in the most extreme of dynamic environments.

5. ACES: AN OPEN, TRANSPARENT, COMMUNITY-WIDE APPROACH TO PRODUCING DATA PRODUCTS AND PAPERS

The ACES collaboration is open to anyone interested in contributing to the project, with membership approved through the management board. The science objectives are facilitated by tasks within four different work packages, led by members of the management team, dedicated to (i) data reduction, (ii) producing the ACES fundamental measurements, (iii) chemistry and physical modelling, and (iv) the unified simulation suite. To ensure complete transparency and fair attribution of credit for key technical tasks, progress within the work packages is tracked using the ACES CMZ public GitHub project (https://github.com/ACES-CMZ). For example, all of the data reduction steps from the delivery of each individual scheduling block, through to production of the final mosaics, can be tracked through separate issues on the data reduction repository (https://github.com/ACES-CMZ/reduction_ACES). This provides a permanent record of the wide range of technical challenges that needed to be overcome, and the dedicated effort from a large number of ACES team members, ALMA staff, contact scientists, technical staff, etc., required to solve the data reduction challenges and produce the final, full-field mosaics. Given the unique challenges associated with the different data products, a full description of the specific data reduction steps are given in the corresponding papers: continuum (Paper II), high spectral resolution spectral windows (Paper III, HCO^+ and HCN), intermediate resolution spectra windows (Paper IV), and low resolution spectral window (Paper V).

All of the ACES data will be accessible through Globus and the ESO data archive. *Details about the distribution of the data, associated meta data, etc., will be added upon acceptance.*

6. ACES: DATA HIGHLIGHTS AND DISCOVERY POTENTIAL

We now show a small selection of the initial ACES data and data products, with the aim of highlighting the power of ACES' combination of angular resolution, spatial dynamic range, sensitivity, spectral resolution and spectral bandwidth. These are selected to illustrate how the ACES data will be used to address the science objectives and understand how global processes set the location, intensity, and timescales for star formation and feedback in the CMZ.

Figures 4, 5, and 6 compare the ACES HNCO data in Figure 1 with other multi-wavelength datasets. Figures 4 and 5 zoom in to the very central region of the Galaxy, containing the arched filaments, the Arches and Quintuplet

stellar clusters, the nuclear stellar cluster, and supermassive black hole, Sgr A*. Figure 6 zooms in to the very massive ($10^5\,M_\odot$), compact (radius of a few pc) G0.253+0.016 molecular cloud, known as the 'Brick'. Throughout the CMZ, the ACES data reliably trace the dense gas structure seen as absorption features at shorter wavelengths.

Figure 7

6.1. *Chemistry and Physical Modeling*

6.1.1. *Molecular benchmarking with known sources*

ACES covers 6 spectral windows in ALMA band 3 at 3 mm (see Table 1 in Ginsburg & ACES Team 2025, for full details). Two of these are high spectral resolution spectral windows ($\sim$0.2 km s^{-1}) devoted to kinematic studies using HCO^+(1–0) and HNCO(4–3) rotational transitions, and will not be discussed in the following. The other four spectral windows cover observed frequencies 85.96–86.43, 86.67–87.13, 97.66–99.54, and 99.56–101.44 GHz at 1.7 to 2.9 km s^{-1} spectral resolution. These observed frequencies cover rotational transitions of many molecular species (see Figs. 8 and 9), allowing for the determination of the physical and chemical properties of the molecular and ionized gas structures from the largest scales ($\sim$100 pc) to individual cores ($\sim$0.05 pc).

The main molecules that can be detected with ACES are dense gas tracers, like HCO^+, HCN, and CS, shock tracers, like SiO, HNCO, and SO, photo-dissociation regions (PDR) tracers, like HCO, ionised gas tracers, like H40α, and hot core tracers, like the v7=1 and v6=1 vibrationally excited lines of HC_3N. Note that the emission from Complex Organic Molecules (COMs) in the CMZ may arise from massive hot cores (such as in the case of Sgr B2 (N); Belloche et al. 2013) or from intermediate-density gas affected by large-scale shocks (Zeng et al. 2018, 2020). The difference between these two components is provided by the measured excitation temperature of the COM emission, which are high for hot cores ($T_{ex}\geq$150 K; Belloche et al. 2013), while they are low for large-scale shocked gas ($T_{ex}\leq$15 K; Zeng et al. 2018, 2020).

Molecular gas in the CMZ is highly turbulent, with supersonic linewidth and shocked material (e.g. Elmegreen & Scalo 2004; Mac Low & Klessen 2004b). A typical example of a chemically rich shocked region in the Galactic Center, without on-going star formation or protostellar activity, is the G+0.693-0.027 (G+0.693 hereafter) molecular cloud, located in the Sgr B2 region, 55″ northeast from Sgr B2(N). In the last 5 years more than 20 new interstellar molecules have been discovered towards this molecular cloud using very sensitive single-dish radio telescope observations (e.g., Rivilla et al. 2021; Jiménez-Serra et al. 2022; San Andrés et al. 2024; Sanz-Novo et al. 2024, 2025). G+0.693 has been recently discovered to harbor a prestellar condensation, hypothesized to be formed from the shock produced by a cloud-cloud collision, which could be the cradle of the next generation of stars in the CMZ (Zeng et al. 2020; Colzi et al. 2022, 2024). ACES high angular resolution observations will allow us to properly map the molecular emission towards this condensation.

In Figs. 8 and 9 we show the observed spectra towards G+0.693 using single-dish observations obtained with the IRAM 30m radiotelescope (see Colzi et al. 2024 for more details on the observations) at the frequencies of SPWs 25, 27, 33, 35. We superimposed the spectra extracted from the ACES cube (12m + ACA 7m + total power) towards the coordinates of the source $\alpha_{J2000} = 17^h47^m22^s$ and $\delta_{J2000} = -28°21'27''$ and from a region matching the size of the IRAM 30m beam at the observed frequency (29″ at 86 GHz).

The match between the single-dish and interferometric observations is very good, indicating the reliability of the data reduction and merging of the different ALMA configurations used to recover the more extended flux. There are some small differences ($<$ 20% in synthesized beam T_{SB}) mainly due to the continuum subtraction, which is not straightforward in the CMZ due to the multiple gas component, especially in the Sgr B2 region (see Paper II by Ginsburg et al., in prep.). In the IRAM 30m spectra, some absorption features appear in very strong lines, like CS at 98 GHz, which are not present in the ACES data. These are due to the subtraction of the off-position while taking the single-dish data.

This comparison with single-dish data shows the potential of ACES data in detecting many molecular species, from simple molecules such as SO, SiO and CS to more complex ones such as CH_3CHO, CH_3SH, and NH_2CN.

Typical molecular excitation temperatures (T_{ex}) towards G+0.693 are of the order of 3-20 K (e.g. Zeng et al. 2018), and thus only the low energy transitions are excited, making the observed spectra less crowded than towards a typical hot molecular core (like the Sgr B2 hot cores, Belloche et al. 2013; Sánchez-Monge et al. 2017; Möller et al. 2025) with $T_{ex} > 100$ K. Taking into account these high excitation conditions, in hot molecular cores other molecular species, apart from those already shown in G+0.693, can be detected, such as H_2CO, CH_3OH, CH_3C_3N, CH_3NCO, HC_3N

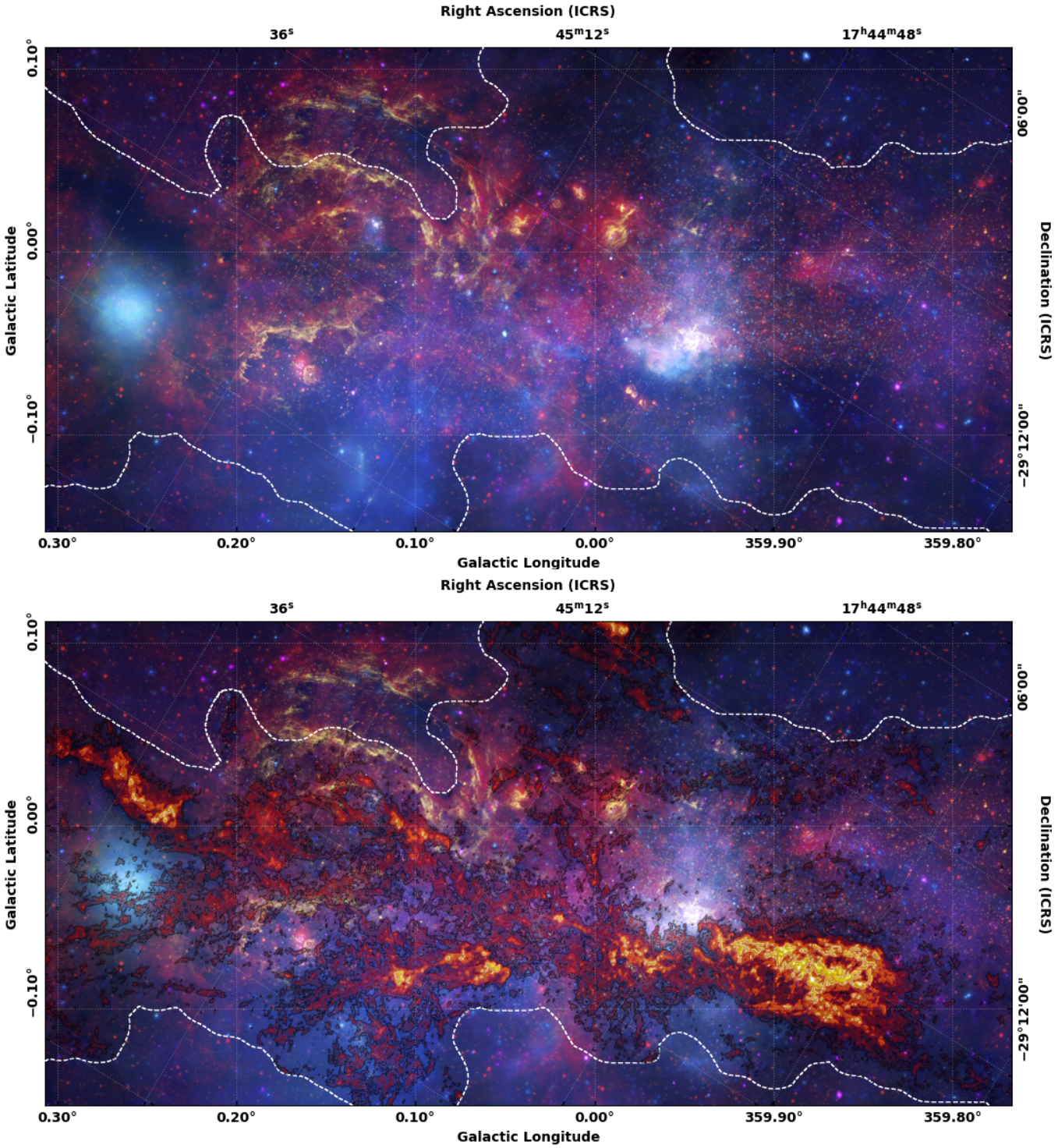

Figure 4. Zoom in to the central few tens of pc of the Galaxy, containing the arched filaments, the Arches and Quintuplet stellar clusters, the nuclear stellar cluster, and supermassive black hole, Sgr A*. The top panel shows a 3-colour composite from the Hubble Space Telescope (HST) Paschen-alpha survey. The bottom panel shows the same region overlaid with the ACES HNCO data from Figure 1.

vibrationally excited, $HC(O)NH_2$. Furthermore, radio recombination lines H40α and H50β are also included in the ACES setup and are well known tracers of ionized gas, e.g., towards HII regions.

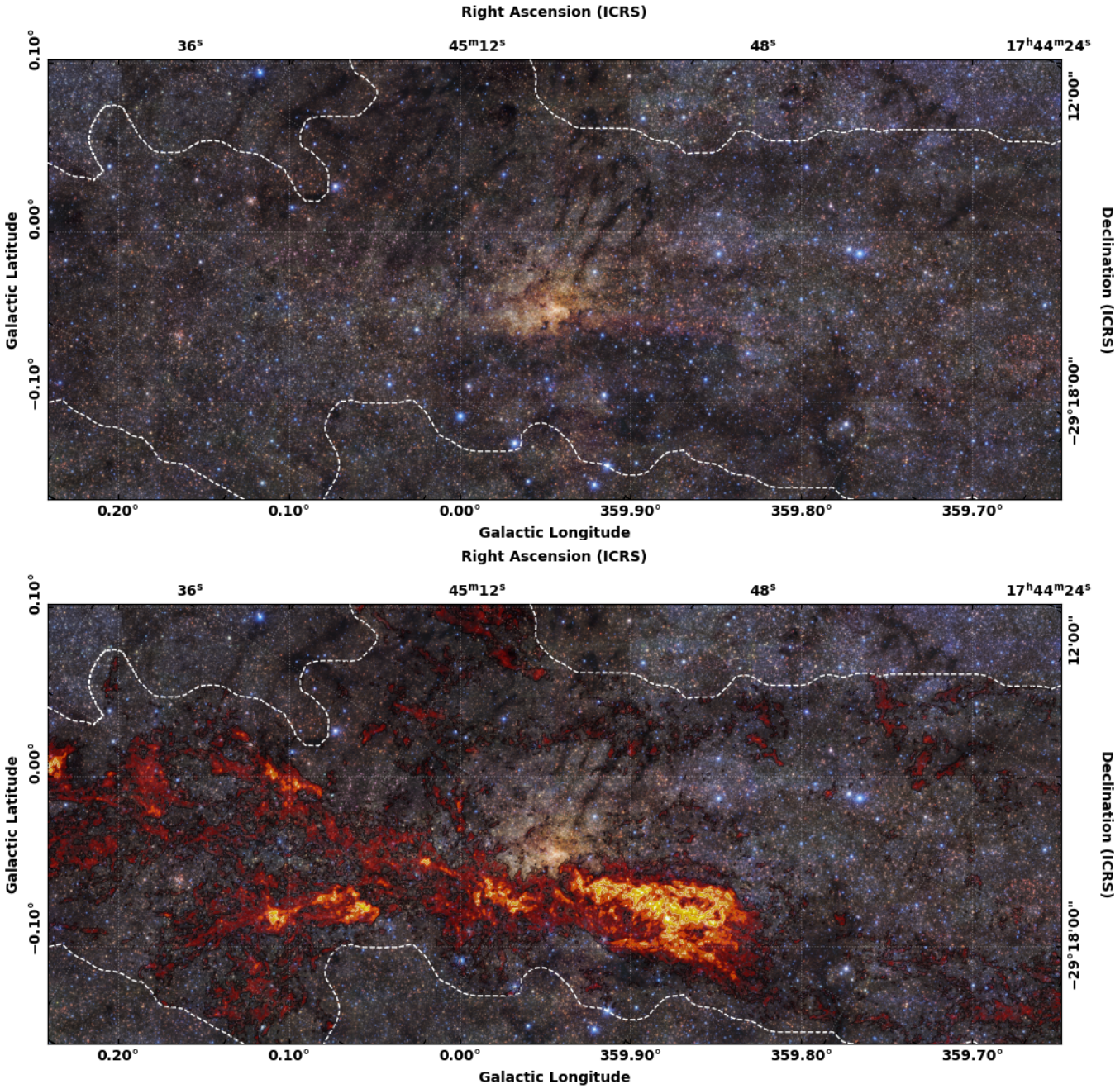

Figure 5. Zoom in to the same region as Figure 4 but with a 3-colour near-IR HAWKI image as the background.

In Table 2 we list the frequencies of the most common rotational transitions of simple molecules present in the ACES setup. In addition, in Table 3, we also list the COMs and COM precursors that we have covered within the frequency setup of ACES. Note we do not list specific transitions for COMs since their excitation and presence in the spectra is highly dependent on the excitation condition of the cloud targeted.

6.1.2. *Astrochemical models*

Astrochemical modelling is vital to interpret the ACES spectral line observations. As part of a wider coordinated effort from multiple research groups, we have recently completed the astrochemical modeling of sources with typical CMZ conditions: a protostellar object designed to resemble cores like those in the Sgr B2 cloud, and C-type shocks

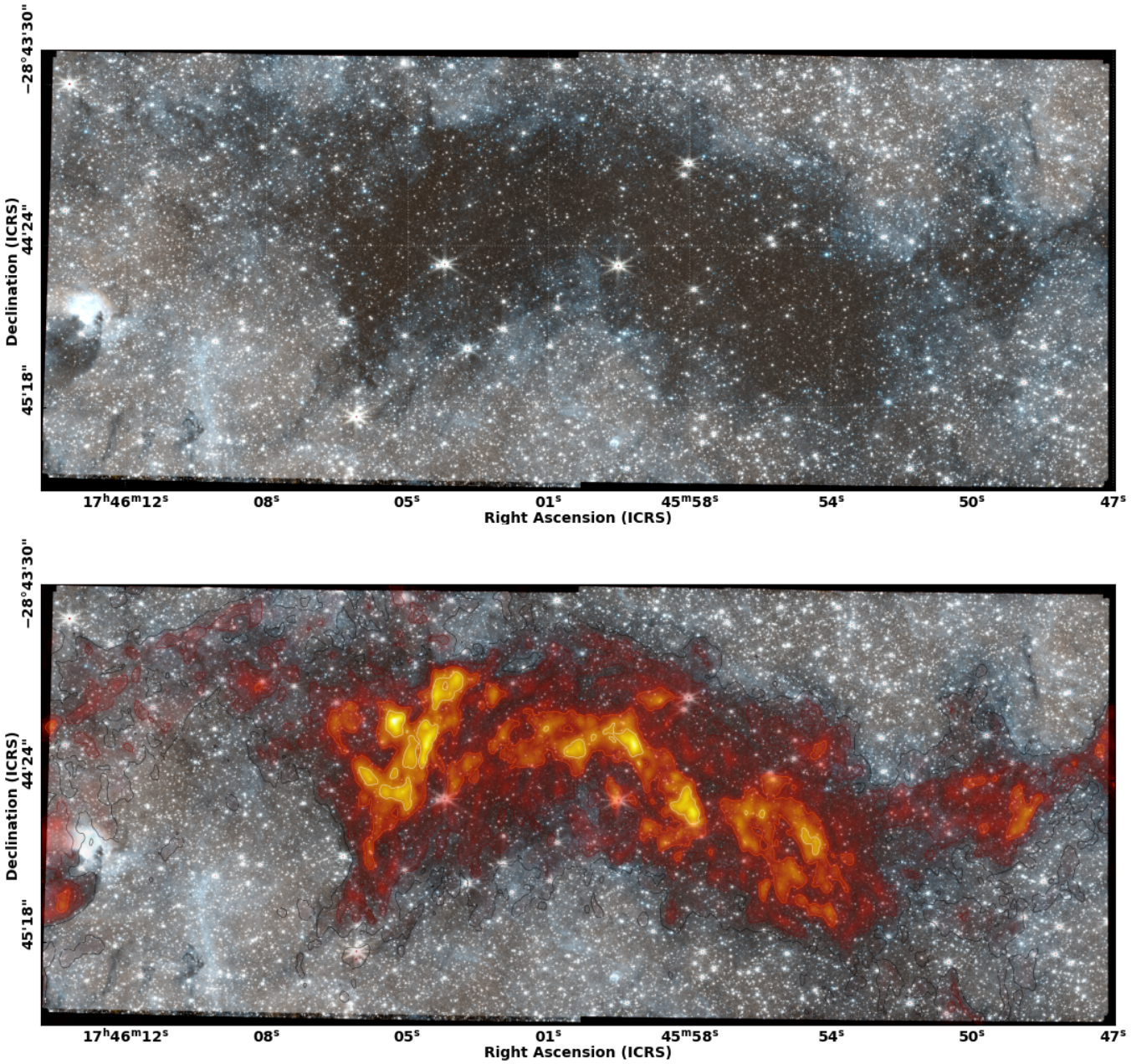

Figure 6. Zoom in to the G0.253+0.016 molecular cloud, known as the 'Brick'. The 3-colour image in the top and bottom panels is from JWST observations reported in (Ginsburg et al. 2023). The bottom panel shows the HNCO data from Figure 1.

occurring during cloud-cloud collisions (e.g., as observed towards G+0.693). Full details of these grids of models simulated using UCLCHEM (Holdship et al. 2017) are given in Dutkowska et al. (2025, in preparation).

In Fig. 10 we show the simulated average chemical abundances for the C-shock models as a function of time. The general trend is that during the shock ($< 10^4$ years) the rise in temperature and density begins almost immediately, leading to general gas phase abundance enhancements. However, in the post-shock stage (after 10^4 years) the gas phase abundances generally decrease. In fact, once the shock passes, the gas and dust cool back to their initial temperatures, the density increases, promoting the freeze-out of species into icy mantles on dust grains.

Predictions for dedicated chemical models over a range of physical conditions expected in the CMZ environment can be found at this link (**link to be added once the paper will be accepted**). These and subsequent models will be vital to interpret the ACES data in the wide range of different physical environments across the Galactic Centre.

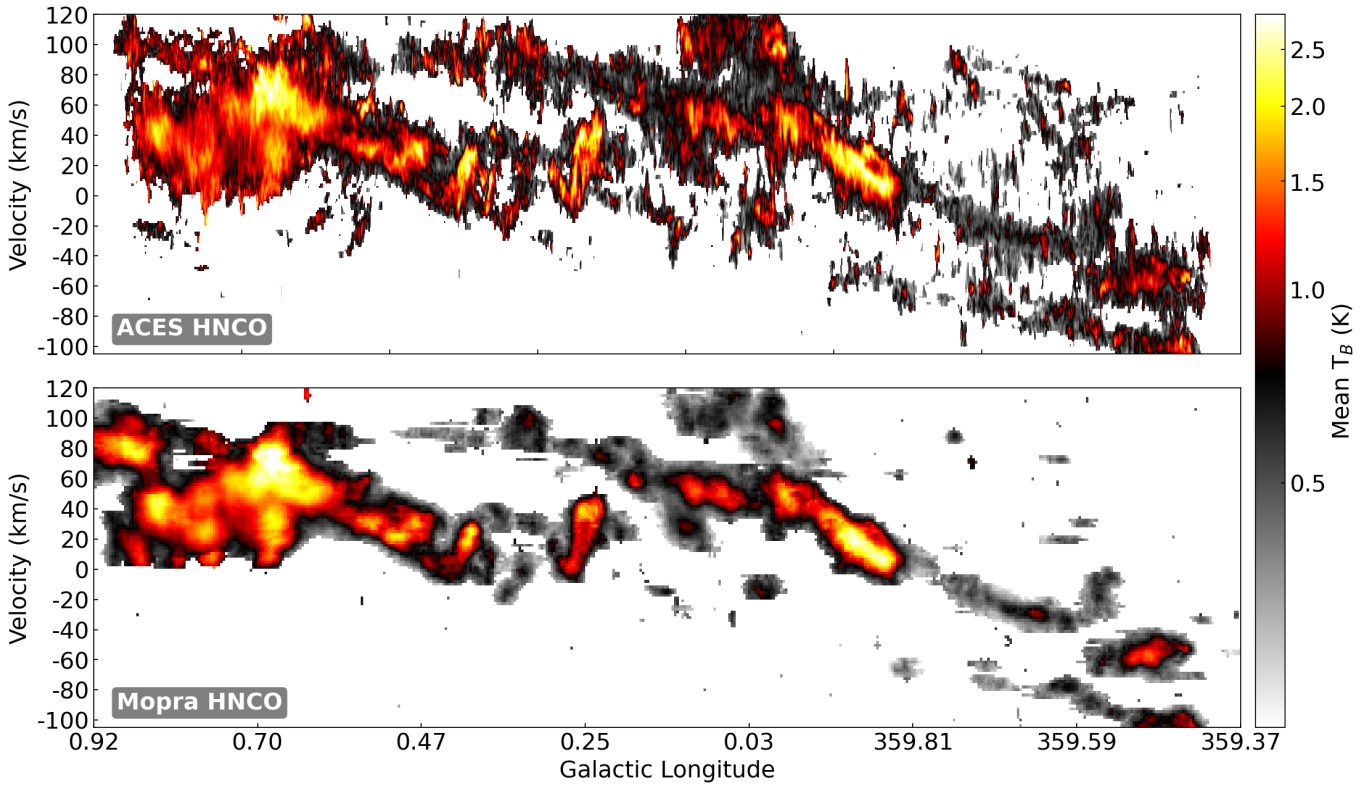

Figure 7. Masked HNCO emission from ACES [top] and the Mopra CMZ survey (Jones et al. 2012) [bottom] summed along Galactic Latitude to show emission velocity as a function of Galactic Longitude. See Walker & ACES Team (2025) for more details on the masking techniques used to create these maps.

Table 3. COMs and COM precursors covered within the ACES frequency setup

COMs families			
O-bearing	N-bearing	S-bearing	C-bearing
CH_3OH, CH_3CHO, CH_3OCHO, H_2CCO, H_3OCH_3, CH_3COCH_3, C_2H_5OH, $HCOCH_2OH$	C_2H_5CN, CH_3NH_2, H_2CCN, CH_3NC, NH_2CN, HC_5N, CH_3NCO, CH_3C_3N	CH_3SH	$^{13}CH_3CCH$

6.2. *ACES Early Science Demonstration: measuring feedback energy and momentum transfer*

A key aspect of ACES Science Objective 1 is to understand how energy and momentum from stellar feedback couples to the surrounding gas and drives the mass flows as a function of size scale and location. Initial science results from ACES data have revealed a striking case of feedback-driven cloud disruption in the CMZ. Nonhebel et al. (2024) present a detailed analysis of the M0.8−0.2 ring, a prominent shell-like molecular cloud complex in the southeastern extension of Sgr B2. Leveraging ACES high angular resolution, sensitivity, spatial dynamic range, and spectral coverage, Nonhebel et al. (2024) determine the complex is an expanding ring of dense, shocked gas with a radius of 6.1 pc, expansion velocity of $\sim$21 km s^{-1}, and a mass approaching 10^6 M$_\odot$. The derived kinetic energy and momentum ($>10^{51}$ erg, $>10^7$ M$_\odot$ km s^{-1}) point to an energetic origin, with detailed radiative transfer modeling and multi-wavelength comparison ruling out early-stage stellar feedback or multiple clustered SNe. Instead, Nonhebel et al. (2024) propose a single high-energy hypernova explosion, likely originating from a runaway massive star, as the most plausible driver of the structure. The inferred energetics challenge canonical models of SNR evolution (e.g. Thornton

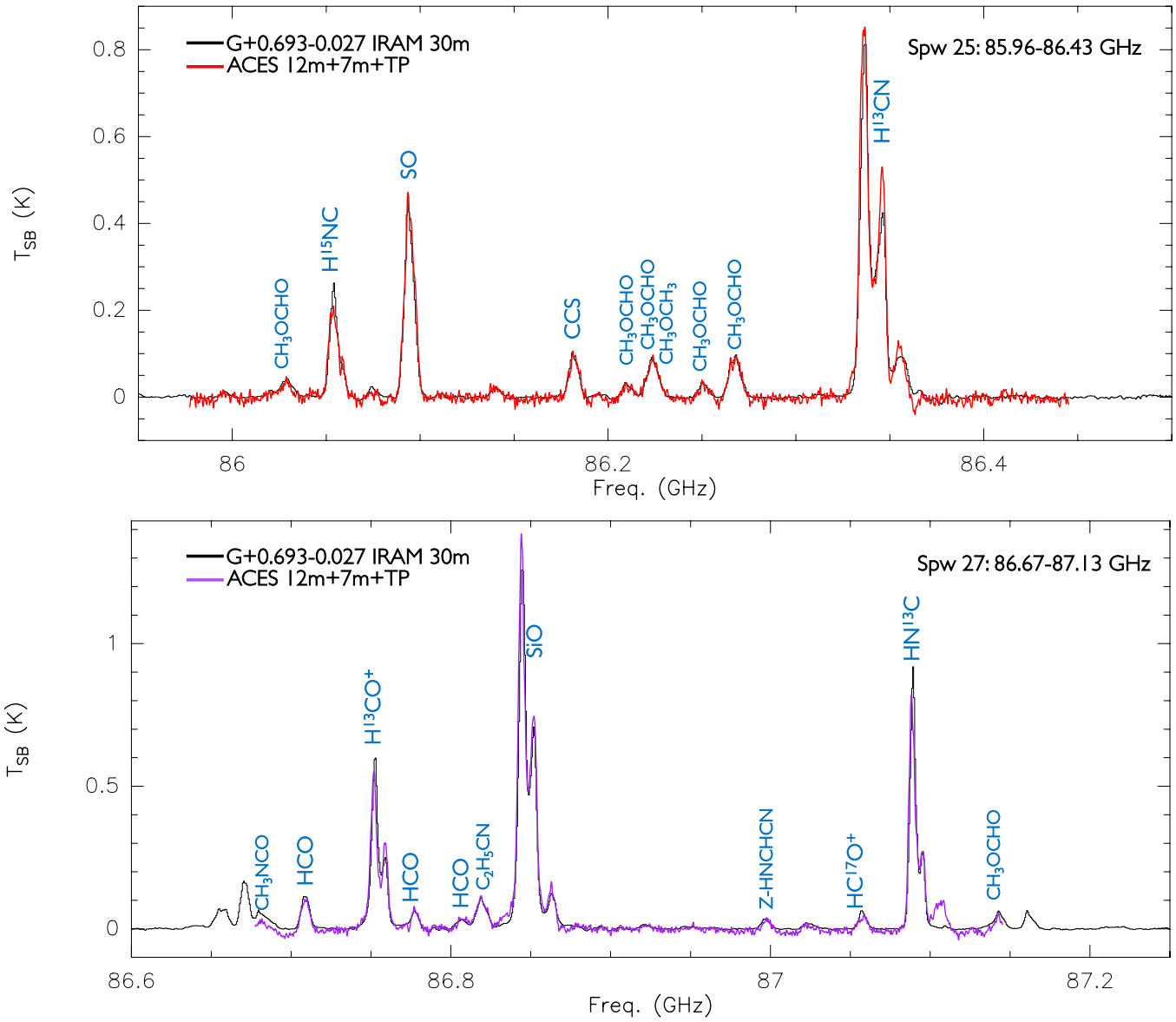

Figure 8. Comparison between the ACES 12m+7m+TP (in red) SPW 25 (*top panel*) and SPW 27 (*bottom panel*) with single-dish spectra obtained with the IRAM 30m (in black) towards the G+0.693 molecular cloud. The blue labels indicate the name of the molecules whose transitions are detected in the observed spectral window.

et al. 1998; Kim et al. 2015) and suggest the need for modified feedback prescriptions in high-density environments like the CMZ.

6.3. *ACES Early Science Demonstration: Disentangling the 3D CMZ geometry*

Sofue et al. (2025) highlight the power of ACES data in separating different velocity structures in the kinematically complex Galactic Centre environment to address Science Objective 2 and understand the 3D structure of the CMZ. Using ACES molecular line data alongside Nobeyama and ASTE observations, Sofue et al. (2025) identify and characterize a nested system of six spiral arms (Arms I–VI) within the Central Molecular Zone (CMZ). These 'arms' appear as coherent, tilted longitude-velocity (LV) ridges in CS and HCN lines, and are interpreted as a sequence of nearly circular, inclined ring-like structures centered on Sgr A*. A new, faint inner arm (Arm V) and the circumnuclear disk (CND; Arm VI) are highlighted, with the ionised minispiral around Sgr A* proposed to constitute an innermost seventh arm.

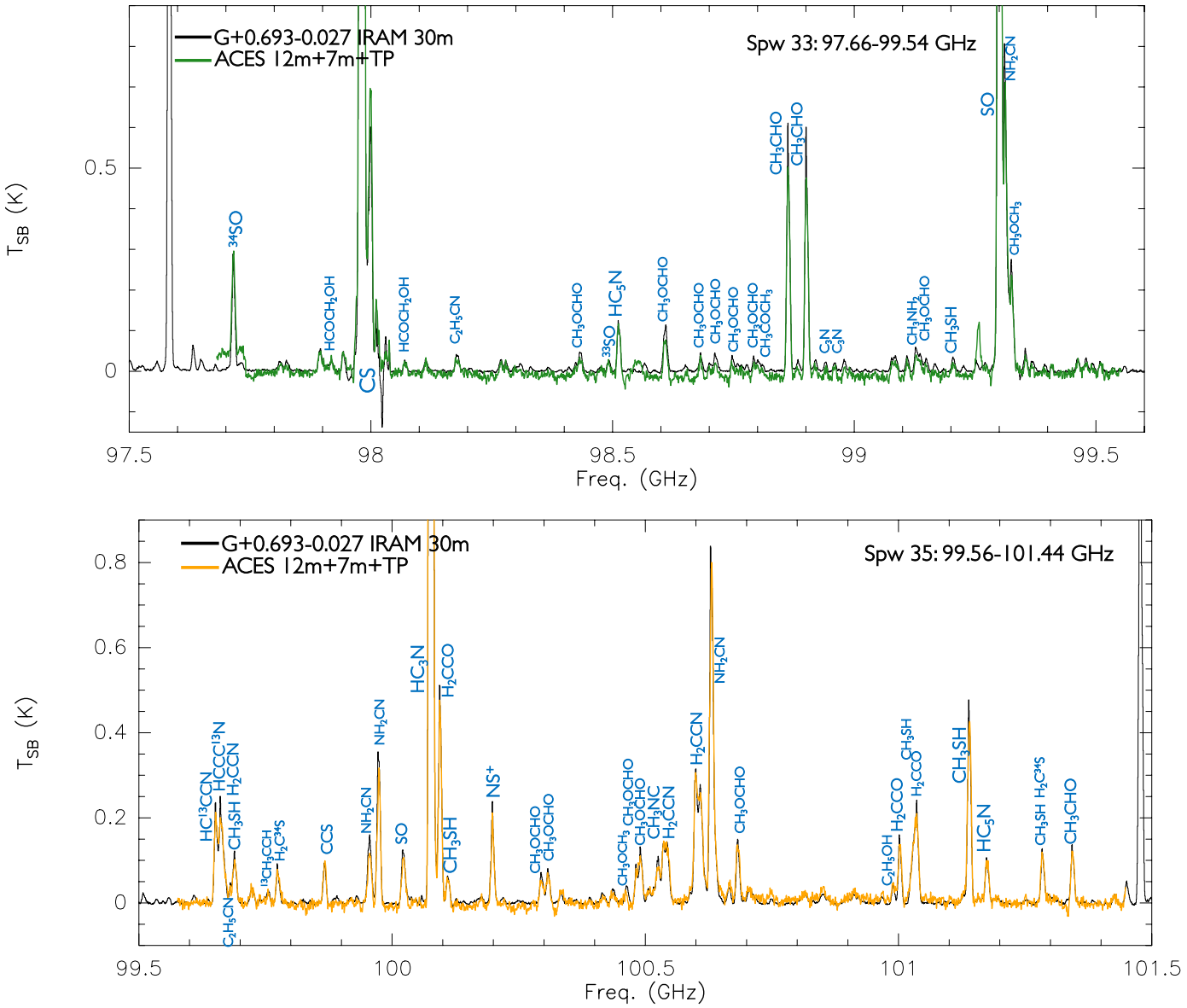

Figure 9. Same as Fig. 8 for ACES spws 33 (*top panel*) and 35 (*bottom panel*).

6.4. *ACES Discovery Potential: Expect the Unexpected*

Any survey, like ACES, which provides orders of magnitude improvements in observational capabilities has the potential to make unexpected discoveries. As part of ACES data quality assessment and early science, Ginsburg et al. (2024) discovered a compact millimeter-bright source near the 50 $\mathrm{km\,s^{-1}}$ cloud, designated G0.02467−0.0727. This object, coined the *Millimeter Ultra-Broad Line Object* (MUBLO), exhibits exceptionally broad molecular line emission (FWHM $\approx 160\,\mathrm{km\,s^{-1}}$) from SO, SO_2, and CS transitions, yet remains remarkably compact ($\lesssim 10^4$ au in diameter). The MUBLO line profiles are well-fit by a Gaussian with no indication of self-absorption or wings, and there is a mild but significant spatial offset between red- and blue-shifted emission, hinting at internal velocity structure.

The continuum emission has a steep spectral index ($\alpha \approx 3.25$), suggesting optically thin dust with a mass of $\sim 50\,M_\odot$ assuming standard CMZ dust properties. Despite the large inferred mass and velocity dispersion, the object shows no sign of high-velocity shocks (e.g., no SiO emission), and no counterpart is detected at infrared, centimeter, or X-ray wavelengths. Its gas appears cold ($T_{\mathrm{LTE}} \approx 13\,\mathrm{K}$), chemically unusual (SO/SiO $\gg 100$), and isolated in projection.

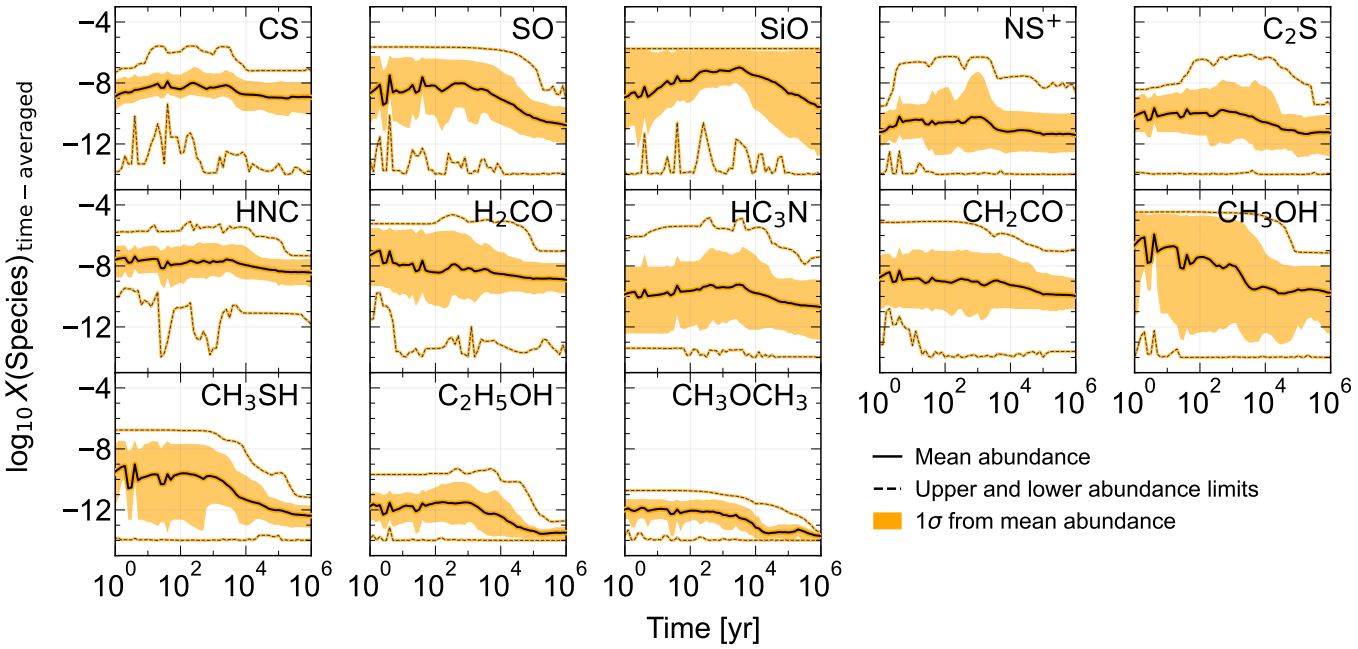

Figure 10. Time-averaged chemical evolution of some species for the C-shock models. Only gas-phase abundances above the observable threshold ($X > 10^{-14}$) are considered. CH_3OH is the most dominant species during the shock phase, while SiO takes over in the post-shock phase. Adapted from Dutkowska et al. (2025, in preparation).

Multiple physical scenarios are evaluated—including a protostellar or explosive outflow, evolved star, stellar merger remnant, high-velocity compact cloud, or gas bound to an intermediate-mass black hole—but none fully explain the observed properties. The MUBLO appears to be an unprecedented and potentially new class of molecular object in the CMZ, highlighting ACES' ability to uncover rare and enigmatic sources through high-resolution, wide-area mapping.

7. CONCLUSIONS

We present an overview of the ALMA CMZ Exploration Survey (ACES), a large-scale ALMA Band 3 program designed to investigate the physical, chemical, and dynamical properties of the molecular gas in the Central Molecular Zone (CMZ) of the Milky Way. By targeting all gas above a column density threshold of $10^{22}\,\mathrm{cm}^{-2}$ in the inner $\sim$100 pc, ACES provides a contiguous, high-resolution view of the star-forming medium across a wide spatial dynamic range, from the scale of the entire CMZ down to individual protostellar cores.

The ACES observational design combines 12m array, 7m ACA, and total power data to recover both compact and extended emission. Its spectral setup enables a comprehensive census of molecular lines tracing a wide variety of physical conditions, from dense and quiescent gas to shocked and ionised regions. ACES thus constitutes an unparalleled dataset for studying the link between large-scale gas flows and the formation of stars in the most extreme environment accessible within our Galaxy.

The scientific motivation for ACES is encapsulated in four key objectives:

- *Determine the mechanisms driving mass flows as a function of size scale and location*: By mapping the kinematic structure and comparing it with simulations, ACES seeks to quantify how orbital dynamics, turbulence, accretion, and feedback shape the gas across the CMZ.

- *Disentangle the 3D geometry of the CMZ*: With high-resolution spectral imaging, ACES aims to resolve overlapping structures and break degeneracies in position–velocity space to reconstruct the spatial configuration of molecular clouds and gas streams.

- *Identify preferred locations for star formation*: ACES will test scenarios in which star formation is triggered at specific dynamical locations (e.g., apocentre, pericentre) or through gas–gas collisions, linking gas properties with embedded stellar populations.

- *Test star formation theories in extreme environments*: By measuring physical quantities such as density, velocity, and temperature, ACES provides fundamental physical parameters of CMZ clouds, including the turbulent Mach number, virial ratio, and turbulence driving mode, as well as the distribution of cores representing the progenitors of high-mass stars, enabling critical tests of theoretical predictions in a regime distinct from the Galactic disc, but representative of starburst and high-redshift galaxies.

We describe how a complementary suite of multi-scale numerical and astrochemical simulations is integrated into the ACES framework to interpret the data and explore the causal links between global dynamics and core-scale star formation. We also highlight several early science results, including the discovery of a compact, chemically unusual object (the MUBLO), a feedback-driven expanding ring structure, and new insights into the orbital structure of the Galactic Centre.

At the same time as publishing this ACES overview paper, we are concurrently publishing four papers describing the continuum data (Ginsburg & ACES Team 2025), high spectral resolution data (Walker & ACES Team 2025), intermediate spectral resolution data (Lu & ACES Team 2025), and broad bandwidth data (Hsieh & ACES Team 2025). We ask anyone using ACES data to cite all of these relevant publications. All ACES data will be publicly released via the ESO archive[1] and Globus[2] upon acceptance, with workflows, reduction scripts, and technical documentation made available through the ACES GitHub repositories[3], ensuring long-term legacy value and enabling broad community engagement.

8. ACKNOWLEDGEMENTS

This paper makes use of the following ALMA data: ADS/JAO.ALMA#2021.1.00172.L. ALMA is a partnership of ESO (representing its member states), NSF (USA) and NINS (Japan), together with NRC (Canada), NSTC and ASIAA (Taiwan), and KASI (Republic of Korea), in cooperation with the Republic of Chile. The Joint ALMA Observatory is operated by ESO, AUI/NRAO and NAOJ.

COOL Research DAO (Chevance et al. 2025) is a Decentralized Autonomous Organization supporting research in astrophysics aimed at uncovering our cosmic origins.

C. Battersby gratefully acknowledges funding from National Science Foundation under Award Nos. 2108938, 2206510, and CAREER 2145689, as well as from the National Aeronautics and Space Administration through the Astrophysics Data Analysis Program under Award "3-D MC: Mapping Circumnuclear Molecular Clouds from X-ray to Radio," Grant No. 80NSSC22K1125.

L.C., I.J-S., and V.M.R. acknowledge support from grant no. PID2022-136814NB-I00 by the Spanish Ministry of Science, Innovation and Universities/State Agency of Research MICIU/AEI/10.13039/501100011033 and by ERDF, UE. I.J.-S. also acknowledges funding from the ERC Consolidator grant OPENS (project number 101125858) funded by the European Union. RSK and SCOG acknowledge financial support from the European Research Council via ERC Synergy Grant "ECOGAL" (project ID 855130), from the German Excellence Strategy via the Heidelberg Cluster "STRUCTURES" (EXC 2181 - 390900948), and from the German Ministry for Economic Affairs and Climate Action in project "MAINN" (funding ID 50OO2206). RSK also thanks the 2024/25 Class of Radcliffe Fellows for highly interesting and stimulating discussions.

C. F. acknowledges funding provided by the Australian Research Council (Discovery Project grants DP230102280 and DP250101526), and the Australia-Germany Joint Research Cooperation Scheme (UA-DAAD).

A.S.-M. acknowledges support from the RyC2021-032892-I grant funded by MCIN/AEI/10.13039/501100011033 and by the European Union 'Next GenerationEU'/PRTR, as well as the program Unidad de Excelencia María de Maeztu CEX2020-001058-M, and support from the PID2023-146675NB-I00 (MCI-AEI-FEDER, UE).

The research of KMD and SV is funded by the European Research Council (ERC) Advanced Grant MOPPEX 833460.vii.

M.C. gratefully acknowledges funding from the DFG through an Emmy Noether Research Group (grant number CH2137/1-1).

The authors acknowledge UFIT Research Computing for providing computational resources and support that have contributed to the research results reported in this publication.

[1] http://www.eso.org/ACES (to be updated upon publication)

[2] http://www.globus.org/ACES (to be updated upon publication)

[3] https://github.com/ACES-CMZ

AG acknowledges support from the NSF under grants CAREER 2142300, AAG 2008101, and particularly AAG 2206511 that supports the ACES large program.

D.L.W gratefully acknowledges support from the UK ALMA Regional Centre (ARC) Node, which is supported by the Science and Technology Facilities Council [grant numbers ST/Y004108/1 and ST/T001488/1].

Q. Z. gratefully acknowledges the support from the National Science Foundation under Award No. AST-2206512, and the Smithsonian Institute FY2024 Scholarly Studies Program.

REFERENCES

Bally, J., Aguirre, J., Battersby, C., et al. 2010, ApJ, 721, 137

Barnes, A. T., Longmore, S. N., Battersby, C., et al. 2017, MNRAS, 469, 2263

Barnes, A. T., Longmore, S. N., Dale, J. E., et al. 2020, MNRAS, 498, 4906

Battersby, C., Keto, E., Walker, D., et al. 2020, ApJS, 249, 35, doi: 10.3847/1538-4365/aba18e

Battersby, C., Walker, D. L., Barnes, A., et al. 2024, arXiv e-prints, arXiv:2410.17334, doi: 10.48550/arXiv.2410.17334

—. 2025a, ApJ, 984, 156, doi: 10.3847/1538-4357/adb5f0

—. 2025b, ApJ, 984, 157, doi: 10.3847/1538-4357/adb844

Belloche, A., Müller, H. S. P., Menten, K. M., Schilke, P., & Comito, C. 2013, A&A, 559, A47, doi: 10.1051/0004-6361/201321096

Bertram, E., Glover, S. C. O., Clark, P. C., Ragan, S. E., & Klessen, R. S. 2015, MNRAS, 451, 3679

Binney, J., Gerhard, O. E., Stark, A. A., Bally, J., & Uchida, K. I. 1991, MNRAS, 252, 210

Böker, T., Falcón-Barroso, J., Schinnerer, E., Knapen, J. H., & Ryder, S. 2008, AJ, 135, 479

Callanan, D., Longmore, S. N., Battersby, C., et al. 2023, MNRAS, 520, 4760, doi: 10.1093/mnras/stad388

Carey, S. J., Noriega-Crespo, A., Mizuno, D. R., et al. 2009, PASP, 121, 76, doi: 10.1086/596581

Chevance, M., Kruijssen, J. M. D., & Longmore, S. N. 2025, arXiv e-prints, arXiv:2501.13160, doi: 10.48550/arXiv.2501.13160

Churchwell, E., Babler, B. L., Meade, M. R., et al. 2009, PASP, 121, 213, doi: 10.1086/597811

Cicone, C., Maiolino, R., Sturm, E., et al. 2014, A&A, 562, A21, doi: 10.1051/0004-6361/201322464

Clark, P. C., Glover, S. C. O., Ragan, S. E., Shetty, R., & Klessen, R. S. 2013, ApJ, 768, L34

Colzi, L., Martín-Pintado, J., Rivilla, V. M., et al. 2022, ApJL, 926, L22, doi: 10.3847/2041-8213/ac52ac

Colzi, L., Martín-Pintado, J., Zeng, S., et al. 2024, A&A, 690, A121, doi: 10.1051/0004-6361/202451382

Dale, J. E., Kruijssen, J. M. D., & Longmore, S. N. 2019, MNRAS, 486, 3307

Elia, D., Evans, N. J., Soler, J. D., et al. 2025, ApJ, 980, 216, doi: 10.3847/1538-4357/adaeb2

Elmegreen, B. G., & Scalo, J. 2004, ARA&A, 42, 211, doi: 10.1146/annurev.astro.41.011802.094859

Federrath, C., & Klessen, R. S. 2012, ApJ, 761, 156, doi: 10.1088/0004-637X/761/2/156

Federrath, C., Rathborne, J. M., Longmore, S. N., et al. 2016, ApJ, 832, 143

Ginsburg, A., & ACES Team. 2025, ApJ, xxx, yyy

Ginsburg, A., Henkel, C., Ao, Y., et al. 2016, A&A, 586, A50

Ginsburg, A., Bally, J., Barnes, A., et al. 2018, ApJ, 853, 171

Ginsburg, A., Heyer, M., Ao, Y., et al. 2020, ApJS, 248, 24

Ginsburg, A., Barnes, A. T., Battersby, C. D., et al. 2023, ApJ, 959, 36, doi: 10.3847/1538-4357/acfc34

Ginsburg, A., Bally, J., Barnes, A. T., et al. 2024, ApJL, 968, L11, doi: 10.3847/2041-8213/ad47fa

GRAVITY Collaboration, Abuter, R., Amorim, A., et al. 2018, A&A, 615, L15

Harrison, C. M. 2017, Nature Astronomy, 1, 0165, doi: 10.1038/s41550-017-0165

Hatchfield, H. P., Sormani, M. C., Tress, R. G., et al. 2021, ApJ, 922, 79, doi: 10.3847/1538-4357/ac1e89

Hatchfield, H. P., Battersby, C., Keto, E., et al. 2020, ApJS, 251, 14, doi: 10.3847/1538-4365/abb610

He, Y. X., Zhou, J. J., Esimbek, J., et al. 2021, ApJ, 908, L33

Heckman, T. M., & Best, P. N. 2014, ARA&A, 52, 589, doi: 10.1146/annurev-astro-081913-035722

Hennebelle, P., & Chabrier, G. 2011, ApJL, 743, L29, doi: 10.1088/2041-8205/743/2/L29

Hennebelle, P., & Chabrier, G. 2013, ApJ, 770, 150

Henshaw, J. D., Barnes, A. T., Battersby, C., et al. 2023, in Astronomical Society of the Pacific Conference Series, Vol. 534, Protostars and Planets VII, ed. S. Inutsuka, Y. Aikawa, T. Muto, K. Tomida, & M. Tamura, 83, doi: 10.48550/arXiv.2203.11223

Henshaw, J. D., Longmore, S. N., Kruijssen, J. M. D., et al. 2016, MNRAS, 457, 2675

Heywood, I., Camilo, F., Cotton, W. D., et al. 2019, Nature, 573, 235, doi: 10.1038/s41586-019-1532-5

Heywood, I., Rammala, I., Camilo, F., et al. 2022, ApJ, 925, 165, doi: 10.3847/1538-4357/ac449a

Holdship, J., Viti, S., Jiménez-Serra, I., Makrymallis, A., & Priestley, F. 2017, AJ, 154, 38, doi: 10.3847/1538-3881/aa773f

Hopkins, P. F. 2013, MNRAS, 430, 1653

Hsieh, P.-Y., & ACES Team. 2025, ApJ, xxx, yyy

Hunter, G. H., Sormani, M. C., Beckmann, J. P., et al. 2024, A&A, 692, A216, doi: 10.1051/0004-6361/202450000

Jiménez-Serra, I., Rodríguez-Almeida, L. F., Martín-Pintado, J., et al. 2022, A&A, 663, A181, doi: 10.1051/0004-6361/202142699

Jones, P. A., Burton, M. G., Cunningham, M. R., et al. 2012, MNRAS, 419, 2961, doi: 10.1111/j.1365-2966.2011.19941.x

Kim, C.-G., Ostriker, E. C., & Raileanu, R. 2015, ApJ, 815, 67, doi: 10.1088/0004-637X/815/1/67

Klessen, R. S., & Glover, S. C. O. 2016, Saas-Fee Advanced Course, 43, 85, doi: 10.1007/978-3-662-47890-5_2

Krieger, N., Ott, J., Beuther, H., et al. 2017, ApJ, 850, 77

Kruijssen, J. M. D., Dale, J. E., & Longmore, S. N. 2015, MNRAS, 447, 1059

Kruijssen, J. M. D., & Longmore, S. N. 2013, MNRAS, 435, 2598

Kruijssen, J. M. D., Longmore, S. N., Elmegreen, B. G., et al. 2014, MNRAS, 440, 3370

Kruijssen, J. M. D., Dale, J. E., Longmore, S. N., et al. 2019, MNRAS, 484, 5734

Krumholz, M. R., & Kruijssen, J. M. D. 2015, Mon. Not. R. Astron. Soc., 453, 739

Krumholz, M. R., Kruijssen, J. M. D., & Crocker, R. M. 2017, Mon. Not. R. Astron. Soc., 466, 1213

Krumholz, M. R., & McKee, C. F. 2005, ApJ, 630, 250, doi: 10.1086/431734

Lada, C. J., Forbrich, J., Lombardi, M., & Alves, J. F. 2012, ApJ, 745, 190, doi: 10.1088/0004-637X/745/2/190

Law, C. J., Yusef-Zadeh, F., Cotton, W. D., & Maddalena, R. J. 2008, ApJS, 177, 255, doi: 10.1086/533587

Leroy, A. K., Bolatto, A. D., Ostriker, E. C., et al. 2018, ApJ, 869, 126

Lipman, D., Battersby, C., Walker, D. L., et al. 2025, ApJ, 984, 159, doi: 10.3847/1538-4357/adb5ee

Longmore, S. N., Kruijssen, J. M. D., Bally, J., et al. 2013a, MNRAS, 433, L15

Longmore, S. N., Bally, J., Testi, L., et al. 2013b, MNRAS, 429, 987

Lu, X., & ACES Team. 2025, ApJ, xxx, yyy

Lu, X., Cheng, Y., Ginsburg, A., et al. 2020, ApJL, 894, L14, doi: 10.3847/2041-8213/ab8b65

Lu, X., Zhang, Q., Kauffmann, J., et al. 2019, ApJ, 872, 171

Lu, X., Li, S., Ginsburg, A., et al. 2021, ApJ, 909, 177, doi: 10.3847/1538-4357/abde3c

Mac Low, M.-M., & Klessen, R. S. 2004a, Reviews of Modern Physics, 76, 125, doi: 10.1103/RevModPhys.76.125

—. 2004b, Reviews of Modern Physics, 76, 125, doi: 10.1103/RevModPhys.76.125

McKee, C. F., & Ostriker, E. C. 2007, ARA&A, 45, 565, doi: 10.1146/annurev.astro.45.051806.110602

Molinari, S., Bally, J., Noriega-Crespo, A., et al. 2011, ApJ, 735, L33

Möller, T., Schilke, P., Sánchez-Monge, Á., & Schmiedeke, A. 2025, A&A, 693, A160, doi: 10.1051/0004-6361/202451274

Murgia, S. 2020, Annual Review of Nuclear and Particle Science, 70, 455, doi: 10.1146/annurev-nucl-101916-123029

Nonhebel, M., Barnes, A. T., Immer, K., et al. 2024, A&A, 691, A70, doi: 10.1051/0004-6361/202451190

Padoan, P., & Nordlund, Å. 2011, ApJ, 730, 40, doi: 10.1088/0004-637X/730/1/40

Petkova, M. A., Kruijssen, J. M. D., Kluge, A. L., et al. 2023a, MNRAS, 520, 2245, doi: 10.1093/mnras/stad229

Petkova, M. A., Kruijssen, J. M. D., Henshaw, J. D., et al. 2023b, MNRAS, 525, 962, doi: 10.1093/mnras/stad2344

Pound, M. W., & Yusef-Zadeh, F. 2018, MNRAS, 473, 2899, doi: 10.1093/mnras/stx2490

Purcell, C. R., Longmore, S. N., Walsh, A. J., et al. 2012, MNRAS, 426, 1972, doi: 10.1111/j.1365-2966.2012.21800.x

Rathborne, J. M., Longmore, S. N., Jackson, J. M., et al. 2015, ApJ, 802, 125

Riquelme, D., Bronfman, L., Mauersberger, R., May, J., & Wilson, T. L. 2010, A&A, 523, A45

Rivilla, V. M., Jiménez-Serra, I., Martín-Pintado, J., et al. 2021, Proceedings of the National Academy of Science, 118, e2101314118, doi: 10.1073/pnas.2101314118

Rodríguez-Fernández, N. J., & Combes, F. 2008, A&A, 489, 115

San Andrés, D., Rivilla, V. M., Colzi, L., et al. 2024, ApJ, 967, 39, doi: 10.3847/1538-4357/ad3af3

Sánchez-Monge, Á., Schilke, P., Schmiedeke, A., et al. 2017, A&A, 604, A6, doi: 10.1051/0004-6361/201730426

Sanz-Novo, M., Rivilla, V. M., Müller, H. S. P., et al. 2024, ApJL, 965, L26, doi: 10.3847/2041-8213/ad3945

Sanz-Novo, M., Rivilla, V. M., Endres, C. P., et al. 2025, ApJL, 980, L37, doi: 10.3847/2041-8213/adafa7

Seo, W.-Y., & Kim, W.-T. 2013, ApJ, 769, 100, doi: 10.1088/0004-637X/769/2/100

Sofue, Y., Oka, T., Longmore, S. N., et al. 2025

Sormani, M. C., & Barnes, A. T. 2019, MNRAS, 484, 1213

Sormani, M. C., Tress, R. G., Glover, S. C. O., et al. 2020, MNRAS, 497, 5024

Stuber, S. K., Schinnerer, E., Williams, T. G., et al. 2023, A&A, 676, A113, doi: 10.1051/0004-6361/202346318

Terrier, R., Clavel, M., Soldi, S., et al. 2018, A&A, 612, A102

Thornton, K., Gaudlitz, M., Janka, H.-T., & Steinmetz, M. 1998, ApJ, 500, 95, doi: 10.1086/305704

Tress, R. G., Sormani, M. C., Glover, S. C. O., et al. 2020, MNRAS, 499, 4455

Tress, R. G., Sormani, M. C., Girichidis, P., et al. 2024, A&A, 691, A303, doi: 10.1051/0004-6361/202450035

Veilleux, S., Cecil, G., & Bland-Hawthorn, J. 2005, ARA&A, 43, 769, doi: 10.1146/annurev.astro.43.072103.150610

Walker, D., & ACES Team. 2025, ApJ, xxx, yyy

Walker, D. L., Longmore, S. N., Bastian, N., et al. 2015, MNRAS, 449, 715, doi: 10.1093/mnras/stv300

Walker, D. L., Longmore, S. N., Zhang, Q., et al. 2018, MNRAS, 474, 2373, doi: 10.1093/mnras/stx2898

Walker, D. L., Longmore, S. N., Bally, J., et al. 2021, MNRAS, 503, 77, doi: 10.1093/mnras/stab415

Walker, D. L., Battersby, C., Lipman, D., et al. 2025, ApJ, 984, 158, doi: 10.3847/1538-4357/adb5ef

Walsh, A. J., Breen, S. L., Britton, T., et al. 2011, MNRAS, 416, 1764, doi: 10.1111/j.1365-2966.2011.19115.x

Xu, F., Lu, X., Wang, K., et al. 2025, A&A, 697, A164, doi: 10.1051/0004-6361/202453601

Zeng, S., Jiménez-Serra, I., Rivilla, V. M., et al. 2018, MNRAS, 478, 2962, doi: 10.1093/mnras/sty1174

Zeng, S., Zhang, Q., Jiménez-Serra, I., et al. 2020, MNRAS, 497, 4896, doi: 10.1093/mnras/staa2187

Zhang, S., Lu, X., Ginsburg, A., et al. 2025, ApJL, 982, L10, doi: 10.3847/2041-8213/adb30b

APPENDIX

A. ACCESSING ACES DATA

Here we will provide detailed instructions on how to access the data.

B. GALACTIC CENTRE OVERVIEW FIGURE

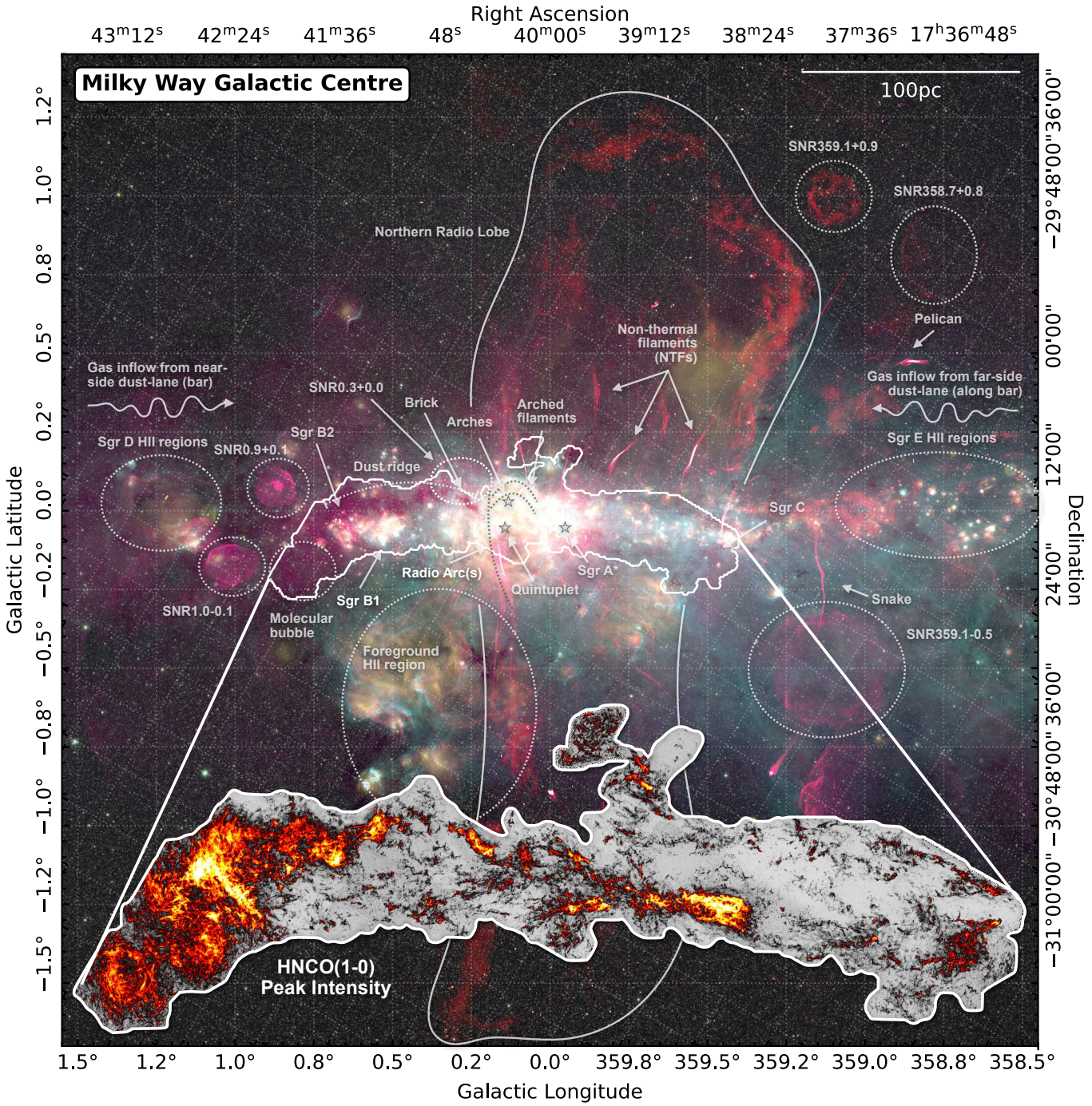

Figure 11. Finding chart for the Galactic Center. A colour composite of the 4.5 μm (white) and 8 μm (green) emission from the Spitzer GLIMPSE survey (Churchwell et al. 2009), 24 μm (yellow) emission from the Spitzer MIPSGAL survey (Carey et al. 2009), and 20 cm (red) emission observed by MeerKAT (Heywood et al. 2019, 2022) and the Green Bank Telescope (GBT; Law et al. 2008). Overlaid are labels highlighting several features of interest across the Galactic Centre, including the central few 100 pc known as the Central Molecular Zone (CMZ). Overlaid as a white contour is the coverage of the ACES survey (see Fig. 2). The background image for this Figure is adapted from Henshaw et al. 2023.